Remote Sensing of Environment 143 (2014) 154–170

Contents lists available at ScienceDirect

Remote Sensing of Environment

journal homepage: www.elsevier.com/locate/rse

Remotely sensed trends in the phenology of northern high latitude terrestrial vegetation, controlling for land cover change and vegetation type

C. Jeganathan [a,*], J. Dash [b], P.M. Atkinson [b]

[a] Department of Remote Sensing, Birla Institute of Technology (BIT), Mesra, Ranchi 835215, Jharkhand, India
[b] Global Environmental Change and Earth Observation Research Group, Geography and Environment, University of Southampton, Southampton SO17 1BJ, United Kingdom

ARTICLE INFO

Article history:
Received 1 June 2013
Received in revised form 25 November 2013
Accepted 25 November 2013
Available online 21 January 2014

Keywords:
NDVI
Phenology
Start of season
End of season
Northern latitude
Terrestrial vegetation
Global warming
Remote sensing

ABSTRACT

Trends in the start or end of growing season (SOS, EOS) of terrestrial vegetation reported previously as latitudinal averages limit the ability to investigate the effects of land cover change and species-wise conditioning on the presented vegetation phenology information. The current research provided more reliable estimates of the trends in the annual growth pattern of terrestrial vegetation occurring at latitudes greater than 45°N. 25 years of satellite-derived Normalised Difference Vegetation Index (GIMMS NDVI) was used and reliable vegetated pixels were analysed to derive the SOS and EOS. The rate of change in SOS and EOS over 25 years was estimated, aggregated and scrutinised at different measurement levels: a) vegetation type, b) percentage vegetative cover, c) core area, d) percentage forest cover loss, and e) latitude zones. The research presents renewed and detailed estimates of the trends in these phenology parameters in these strata. In the >45°N zone, when only reliable pixels were considered, there was an advancement of −0.58 days yr^{-1} in SOS and a delay of +0.64 days yr^{-1} in EOS. For homogeneous vegetated areas (91–100% cover at 8 km spatial resolution) the 55–65°N zone showed the maximum change with −1.07 days yr^{-1} advancement in SOS for *needle leaved deciduous vegetation*, and −1.06 days yr^{-1} delay in EOS for *broad leaved deciduous vegetation*. Overall, the increasing trend in EOS during senescence (September to November) was greater in magnitude than the decreasing trend in SOS during spring (March to May) and the change in EOS was more consistent and greater than that in SOS.

1. Introduction

Recent global surface temperature records, after incorporating several corrections, confirm an increasing trend in the rate of global warming, with the 12 month running mean temperature reaching a record high in 2010 (Hansen, Ruedy, Sato, et al., 2010). Such strongly increasing trends suggest anthropogenically-induced changes in climate. Although climate is the manifestation of many global processes occurring due to the coupling of land, ocean and atmospheric phenomena, human growth and development in the 20th century has been a major factor in altering the climate system. The human population is growing enormously at a rate of ~1 billion every 12 years (1.5 billion in 1900; 3 billion in 1960; 5 billion in 1987; 6.1 billion in 2000; 6.9 billion in mid-2011) with a daily rate of 200,000 people (Weeks, 2012) and, hence, human needs are growing commensurately, influencing the land, oceans and atmosphere and hence, the global climate. Within the terrestrial biosphere the effects of a changing climate have already been observed through changes in the physiology, distribution, phenology and biodiversity of vegetative species (Cleland, Chuine, Menzel, et al., 2007; Hughes, 2000; Parmesan & Yohe, 2003; Penuelas & Filella, 2001; Thuiller, Lavorel, Araujo, et al., 2005). Hansen, Stehman, and Potapov (2010), using satellite sensor data from 2000 to 2005, revealed a massive loss of gross global forest cover (~1 million km^2) due to natural and human-made disturbances, with the boreal biome recording the largest loss. The boreal ecosystem represents one-third of global forest cover with a rich biodiversity and it plays a significant role in the carbon cycle (Bradshaw, Warkentin, & Sodhi, 2009). Hence, it is important to characterise the spatio-temporal variation in photosynthetic activity driven by vegetation growth in this ecosystem. In addition to the availability of photosynthetically active radiation (PAR), the growth cycle of natural vegetation in the tropical regions is driven mainly by rainfall and in the northern latitudes temperature is the dominant driver (Gong & Ho, 2003; Korner & Basler, 2010; Tanja, Berninger, Vesala, et al., 2003). Hence, global warming is expected to increase the photosynthetic activity of higher northern latitude vegetation and this was also predicted through models (Piao, Friedlingstein, Ciais, et al., 2006). Many studies also confirmed an earlier green-up and longer duration of greening season associated with increasing temperature, for example, over northern lands (>50°N) (Xu, Myneni, Chapin, et al., 2013), in western Siberia and

* Corresponding author. Tel.: +91 8987630041; fax: +91 651 2275401.
E-mail addresses: jegan_iirs@yahoo.com (C. Jeganathan), j.dash@soton.ac.uk (J. Dash), pma@soton.ac.uk (P.M. Atkinson).

0034-4257/$ – see front matter © 2014 Elsevier Inc. All rights reserved.
http://dx.doi.org/10.1016/j.rse.2013.11.020

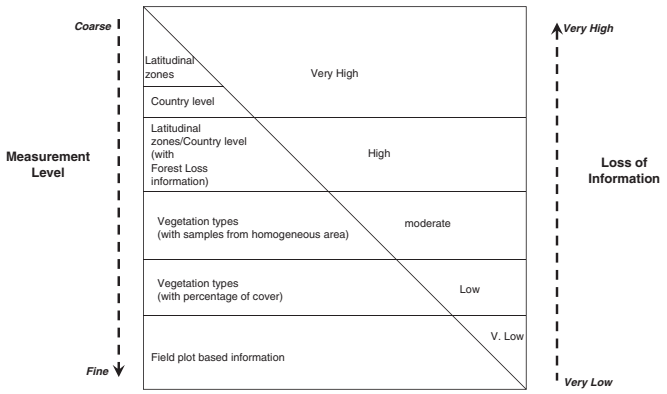

Fig. 1. Conceptual model showing variation of uncertainty in SOS and EOS estimation at different measurement levels.

Eastern Europe (Forbes, Fauria, & Zetterberg, 2010), Europe (Vitasse, Francois, Delpierre, et al., 2011), Eurasia (Delbart, Picard, Le Toans, et al., 2008), North America (Verbyla, 2008; Wang, Piao, Ciais, et al., 2011) and across the globe (Myneni, Keeling, Tucker, et al., 1997; Nemani, Keeling, Hashimoto, et al., 2003).

Tucker, Fung, Keeling and Gammon (1986) established a relationship between satellite-derived vegetation indices and atmospheric CO_2 concentrations. Keeling, Chin and Whorf (1996) hypothesised a lengthening of the plant growth cycle from observed changes in the atmospheric CO_2 cycle. Through the first satellite-based study of the topic, Myneni et al. (1997) confirmed that an increased plant growth in the northern high latitudes correlated positively with increasing atmospheric carbon dioxide during 1981 to 1991. These studies triggered a new research focus using satellite-derived time-series vegetation indices to predict vegetation phenology (i.e., the pattern of vegetation growth dynamics) and linking phenology with many climatic and environmental parameters. Jeong, Ho, Gim, et al. (2011; see Table 1, pp. 2386), Julien and Sobrino (2009; see Table 1, pp. 3509) and Linderholm (2006; see Table 1, pp. 2) listed studies dealing with long-term changes in vegetation growing season, but of those only a few have examined global level changes in the start of season (i.e., greening) (SOS) or end of season (i.e., senescence) (EOS). On a hemispheric scale, Myneni et al. (1997) revealed −0.727 days yr^{-1} change in SOS during 1981 to 1991, Julien and Sobrino (2009) revealed −0.38 days yr^{-1} change in SOS and

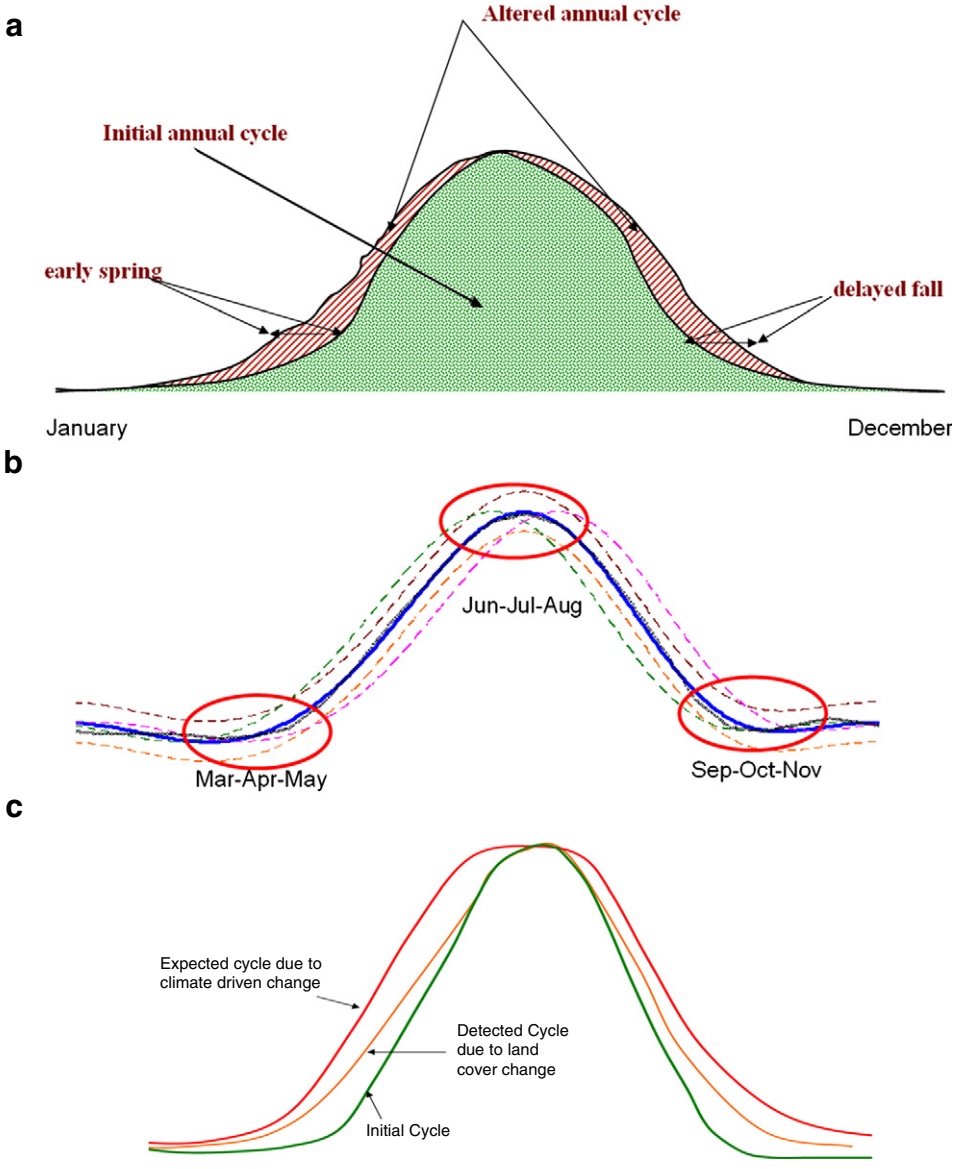

Fig. 2. Conceptual variation in vegetation growth cycle: a) influence due to climate change, b) possible variation in the cycle and c) variation due to land cover change.

Table 1
Mean statistical trend of SOS and EOS over different latitude zones.

Latitudinal zones	Using all high quality pixels		Using only significant pixels	
	SOS trend (days yr^{-1})	EOS trend (days yr^{-1})	SOS trend (days yr^{-1})	EOS trend (days yr^{-1})
Above 45°N	−0.13**	+0.17**	−0.58***	+0.64***
	(r^2 = 0.21)	(r^2 = 0.19)	(r^2 = 0.81)	(r^2 = 0.74)
	(n = 682,105)	(n = 682,105)	(n = 63,114)	(n = 57,450)
45 to 55°N	−0.075~	+0.19**	−0.31***	+0.68***
	(r^2 = 0.09)	(r^2 = 0.24)	(r^2 = 0.59)	(r^2 = 0.77)
	(n = 290,102)	(n = 290,102)	(n = 27,872)	(n = 22,699)
55 to 65°N	−0.19**	+0.20**	−0.86***	+0.71***
	(r^2 = 0.18)	(r^2 = 0.16)	(r^2 = 0.76)	(r^2 = 0.68)
	(n = 306,921)	(n = 306,921)	(n = 29,234)	(n = 30,401)
Above 65°N	−0.11~	+0.01~	−0.53***	+0.08~
	(r^2 = 0.09)	(r^2 = 0.00)	(r^2 = 0.71)	(r^2 = 0.03)
	(n = 85,082)	(n = 85,082)	(n = 6008)	(n = 4350)

*** indicates 99% significance, ** indicates 95% significance, ~ indicates no significance and 'n' indicates number of pixels.

+0.45 days yr^{-1} for EOS during 1981 to 2003, and Jeong et al. (2011) revealed −0.2 days yr^{-1} change in SOS and +0.24 days yr^{-1} for EOS during 1981 to 2008. The difference in these results may be due to (a) differences in methodology, (b) differences in the number of years of data used in the studies, or (c) non-linear adaptation, in-phase with climate dynamics, in the actual growth rhythm of vegetation over the years. Jeong et al. (2011) revealed that the trend towards earlier SOS had slowed down in the last decade and it was marginally earlier at −0.02 days yr^{-1} during 2000–2008 compared to −0.29 days yr^{-1} during 1982–1999.

Most of the above regional–global studies used latitudinal averages to report changes in vegetation phenology. While such a coarse-scale representation has the benefit of simplicity, it limits the ability to investigate the effects of land cover change and species-wise conditioning on vegetation phenology. Morisette, Richardson, Knapp, et al. (2009) addressed cross-cutting issues and challenges, and provided a detailed review of global phenological research. Fig. 1 provides a schematic representation of the amount of uncertainty (i.e., loss of information) associated with different measurement levels (i.e., spatial resolution) while estimating SOS and EOS. At a finer spatial resolution, individual plots or tree level information can provide high confidence (very low uncertainty) whereas results presented as latitudinal averages or at country level have greater uncertainty relative to point sampled vegetation phenology on the ground. Earlier studies have not considered the loss of information in vegetation phenology at different measurement levels (e.g., vegetation cover, percentage distribution, latitudinal variation, and forest cover loss).

The current research acknowledges that there is uncertainty associated with globally estimated phenology parameters (e.g., SOS and EOS) and associated trends in those parameters when reported as latitudinal averages. Hence, the objective of this research was to examine the variation in SOS and EOS using freely available Global Inventory Modelling and Mapping Studies (GIMMS) NDVI data from 1982 to 2006 at several measurement levels such as to (a) characterise the variation in vegetation phenology for major vegetation classes and (b) examine the effect of land cover changes (especially forest cover loss) on phenology. Also, the research aimed to reveal more realistic estimates of the trends in SOS and EOS within each latitudinal zone and their sensitivity

Table 2
Trend in SOS and EOS within vegetation types.

Vegetation type (Globcover Class code)	Using all high quality pixels in each class		Using only significant pixels in each class	
	SOS trend (days yr^{-1})	EOS trend (days yr^{-1})	SOS trend (days yr^{-1})	EOS trend (days yr^{-1})
Mosaic vegetation (grassland/shrubland/forest) (50–70%)/cropland (20–50%) (Class 30)	−0.11*	+0.05~	−0.54***	+0.15*
	(r^2 = 0.15)	(r^2 = 0.02)	(r^2 = 0.59)	(r^2 = 0.12)
	(n = 19,365)	(n = 19,365)	(n = 2395)	(n = 1464)
Closed (>40%) broadleaved deciduous forest (>5 m) (Class 50)	−0.07~	+0.27***	−0.27***	+0.95***
	(r^2 = 0.06)	(r^2 = 0.29)	(r^2 = 0.45)	(r^2 = 0.71)
	(n = 52,413)	(n = 52,413)	(n = 5739)	(n = 5841)
Closed (>40%) needleleaved evergreen forest (>5 m) (Class 70)	+0.07~	+0.22**	−0.25***	+0.93***
	(r^2 = 0.03)	(r^2 = 0.25)	(r^2 = 0.36)	(r^2 = 0.79)
	(n = 20,451)	(n = 20,451)	(n = 2050)	(n = 2010)
Open (15–40%) needleleaved deciduous or evergreen forest (>5 m) (Class 90)	−0.13*	+0.13~	−0.73***	+0.60***
	(r^2 = 0.15)	(r^2 = 0.11)	(r^2 = 0.73)	(r^2 = 0.66)
	(n = 297,279)	(n = 297,279)	(n = 27,371)	(n = 25,224)
Closed to open (>15%) mixed broadleaved and needleleaved forest (>5 m) (Class 100)	−0.14**	+0.28**	−0.66***	+1.01**
	(r^2 = 0.22)	(r^2 = 0.25)	(r^2 = 0.82)	(r^2 = 0.74)
	(n = 46,702)	(n = 46,702)	(n = 4359)	(n = 4954)
Mosaic forest or shrubland (50–70%)/grassland (20–50%) (Class 110)	−0.05~	+0.03~	−0.32***	+0.25***
	(r^2 = 0.03)	(r^2 = 0.02)	(r^2 = 0.39)	(r^2 = 0.36)
	(n = 23,609)	(n = 23,609)	(n = 1877)	(n = 1659)

Class 130 — Closed to open (>15%) (broadleaved or needleleaved, evergreen or deciduous) shrubland (<5 m); Class 140 — Closed to open (>15%) herbaceous vegetation (grassland, savannas or lichens/mosses); Class 150 — Sparse (<15%) vegetation; Class 160 — Closed to open (>15%) broadleaved forest regularly flooded (semi-permanently or temporarily) — Fresh or brackish water; Class 170 — Closed (>40%) broadleaved forest or shrubland permanently flooded — Saline or brackish water; Class 180 — Closed to open (>15%) grassland or woody vegetation on regularly flooded or waterlogged soil — Fresh, brackish or saline water.
*** indicates 99% significance, ** indicates 95% significance, * indicates 90% significance, ~ indicates no significance and 'n' indicates number of pixels.

Table 3
Trend in SOS and EOS for vegetation classes at different latitudes using significant pixels alone.

Vegetation class	SOS trend (units in days yr^{-1})			EOS trend (units in days yr^{-1})		
	45–55°N	55–65°N	Above 65°N	45–55°N	55–65°N	Above 65°N
Class 50	−0.26*** (r^2 = 0.38) (n = 3560)	−0.28** (r^2 = 0.22) (n = 2163)	−0.53** (r^2 = 0.25) (n = 16)	+0.62*** (r^2 = 0.60) (n = 2546)	+1.22*** (r^2 = 0.66) (n = 3269)	+0.76*** (r^2 = 0.44) (n = 26)
Class 70	−0.12~ (r^2 = 0.11) (n = 1687)	−0.81*** (r^2 = 0.66) (n = 363)	N.A.	+1.06*** (r^2 = 0.83) (n = 1747)	+0.04~ (r^2 = 0.00) (n = 263)	N.A.
Class 90	−0.05~ (r^2 = 0.02) (n = 5943)	−1.03*** (r^2 = 0.73) (n = 17,183)	−0.50*** (r^2 = 0.63) (n = 4245)	+0.77*** (r^2 = 0.71) (n = 5945)	+0.59*** (r^2 = 0.60) (n = 16,851)	+0.25** (r^2 = 0.17) (n = 2375)
Class 100	−0.56*** (r^2 = 0.68) (n = 1734)	−0.74*** (r^2 = 0.72) (n = 2409)	−0.62*** (r^2 = 0.52) (n = 216)	+1.08*** (r^2 = 0.71) (n = 1932)	+1.09*** (r^2 = 0.67) (n = 2620)	+0.07~ (r^2 = 0.02) (n = 402)

N.A. indicates pixels not available, *** indicates 99% significance, ** indicates 95% significance, * indicates 90% significance, ~ indicates no significance and 'n' indicates number of pixels.

within different vegetation types, different percentages of vegetative cover and different percentages of forest loss.

Recently, Xu et al. (2013) revealed a tight coupling between winter temperature change and associated changes in the vegetation seasonality and their study recommended continued vegetation monitoring over the northern latitudes. Similarly, this research adds continuity and reveals additional information to previously reported global phenological trends and can be considered as an extension of Myneni et al. (1997), Julien and Sobrino (2009) and Jeong et al. (2011).

2. Materials and methods

Normalised difference vegetation index (NDVI) data provided by the Global Inventory Modelling and Mapping Studies (GIMMS) were used. Data representing 25 years from 1982 to 2006 were downloaded from the NASA website (ftp://ftp.glcf.umiacs.umd.edu/glcf/GIMMS/Geographic). The GIMMS data (15 day temporal resolution, 8 km spatial resolution) were created originally using a maximum value compositing technique and corrected for solar zenith angle, atmospheric effects and volcanic aerosols (El Chichon eruption in 1982; Mount Pinatubo eruption in 1991) for the period 1982–1984 and 1991–1994 (Pinzon, 2002; Pinzon, Brown, & Tucker, 2004; Tucker, Pinzon, Brown, et al., 2005).

2.1. Data preparation

To focus on the most reliable NDVI values only those pixels covering natural vegetation were considered. First, non-vegetative pixels (NDVI $\leq$ 0.1) and agricultural pixels were removed from each composite for the 25 years. The agricultural area was selected using the Advanced Very High Resolution Radiometer (AVHRR) global land cover map (8 km spatial resolution) (Hansen, DeFries, Townshend, et al., 2000). It was assumed that the NDVI value for a specific pixel at a given time of year may vary between different years due to changing ground and atmospheric conditions which are not related to vegetation growth. Therefore, the NDVI value at each pixel for a given time period (i.e., a composite layer) was compared to its mean over 25 years and those pixels with a value greater than $\pm 3\sigma$ from the mean were removed. The pixels available at each composite level, after the conditional processing described above, were considered to be of "high quality" and were used in further analysis. The gap produced due to this elimination process in a year was filled with the mean from reliable temporal neighbours prior to converting composite data into daily data while extracting the phenological parameters.

2.2. Temporal NDVI analysis

Conceptually, in a spatially static ecosystem, an increase in mean temperature is expected to induce an earlier SOS and delayed EOS especially in the northern high latitudinal regions (Fig. 2a) (Jeong et al., 2011). However, there may be other ways in which plants may adapt to changing climatic conditions such as translation of the growth period in either direction (termed as "translational ecosystem"), scaling or non-linear alteration of the growth cycle (termed as "scaling ecosystem") (Fig. 2b, c). Such changes may also occur as spatially migrating ecosystems. All such climate induced alterations, irrespective of type,

Table 4
Trend in SOS and EOS within significant pixels having 91 to 100% tree cover.

Vegetation class	SOS trend (units in days yr^{-1})			EOS trend (units in days yr^{-1})		
	45–55°N	55–65°N	Above 65°N	45–55°N	55–65°N	Above 65°N
Class 50	+0.26** (r^2 = 0.24) (n = 183)	+0.08~ (r^2 = 0.02) (n = 77)	N.A.	−0.25~ (r^2 = 0.11) (n = 199)	+1.06*** (r^2 = 0.52) (n = 95)	N.A.
Class 70	+0.35*** (r^2 = 0.46) (n = 58)	N.A.	N.A.	+1.323*** (r^2 = 0.75) (n = 78)	N.A.	N.A.
Class 90	+0.21*** (r^2 = 0.26) (n = 1115)	−1.07*** (r^2 = 0.53) (n = 5217)	−0.51*** (r^2 = 0.55) (n = 707)	+0.67*** (r^2 = 0.67) (n = 911)	+0.41*** (r^2 = 0.55) (n = 4892)	−0.03~ (r^2 = 0.00) (n = 221)
Class 100	−0.06~ (r^2 = 0.01) (n = 8)	−0.37~ (r^2 = 0.07) (n = 19)	−0.78** (r^2 = 0.18) (n = 7)	+0.69*** (r^2 = 0.28) (n = 12)	+0.36* (r^2 = 0.14) (n = 6)	−0.85*** (r^2 = 0.32) (n = 14)

N.A. indicates pixels not available, *** indicates 99% significance, ** indicates 95% significance, * indicates 90% significance, ~ indicates no significance and 'n' indicates number of pixels.

Fig. 3. Temporal variation in seasonal amplitude (July–August average) at different latitudinal zones.

produce changes in NDVI value during the major growth phases: greening (Mar–Apr–May), peak growth (Jun–Jul–Aug) and senescence (Sep–Oct–Nov), and information on such changes can be used to characterise the type of response. Hence, the variation in mean NDVI value was analysed during these different vegetation growth phases in spring, summer and winter. The percentage change from 1982 to 2006 was calculated by fitting a linear regression model to the mean NDVI value plotted against year. Then, the significance of the fitted model was tested and the pixels which are significant (95% confidence level) were extracted to determine the spatial distribution of reliable change areas during these three growing phases.

2.3. SOS and EOS extraction

To estimate the SOS and EOS, annual NDVI (15 day composite; 24 bands; high quality pixels; as explained in Section 2.1) was first interpolated to provide a daily dataset (assuming linear trend between composites) and then smoothed using the Fourier method (Verhoef, Menenti, & Azzali, 1996; Roerink, Menenti, & Verhoef, 2000; Jakubauskas, Legates, & Kastens, 2001; Moody & Johnson, 2001; Wagenseil & Samimi, 2006; Geerken, 2009; Dash, Jeganathan, & Atkinson, 2010; Jeganathan, Dash, & Atkinson, 2010a, 2010b; Atkinson, Jeganathan, Dash, & Atzberger, 2012). The first six Fourier components (mean + five harmonics) were used because they reproduced satisfactorily the original annual growth profile. The smoothed data were searched iteratively (both sides from the peak) to estimate the SOS and EOS. The SOS is the day of year (DOY) where the first derivative (i.e., difference in NDVI between two consecutive days) exceeds a user-specified NDVI threshold consistently for four days during the growing period in spring and similarly EOS is the DOY at the end of senescence obeying the same criterion in reverse. A derivative threshold of 3.33 days^{-1} (using the GIMMS NDVI scale) was found to be reliable and applied to all years to extract SOS and EOS. The temporal trend in the extracted SOS and EOS was analysed over 25 years by fitting a regression model. Then, we estimated the significance of the fitted model and the pixels which were significant (95% confidence level) were extracted and these pixels were referred as "significant" pixels. The "high quality" pixels (Section 2.1) and "significant" pixels extracted through trend analysis were used to characterise the changes in the resultant phenology variables and their trends in further analysis. Finally, the estimated SOS and EOS were averaged within each measurement level (see Section 2.4) and analysed at these different levels. The averaging effect may alter the resultant SOS and EOS values in each year, and hence the significance of the rate of change was again calculated to provide a reliability check.

2.4. Stratification-based analysis

Both the mean NDVI and estimated phenology parameters were analysed at five different measurement levels: (a) by latitudinal zone, (b) by percentage forest loss, (c) by vegetation type, (d) within "core" areas of each vegetation type, and (e) for different percentages of each vegetation type.

2.5. Effect of land cover change

A change in land cover within a pixel over time may result in changes in the observed vegetation phenological cycle. For example, if over the 25 years the proportion of a forest within a pixel was changed due to deforestation or fire, then this could alter the phenological signal (Fig. 2c). If the changes in land cover were not considered for these pixels then this may lead to false inferences about the effect of climate change on the observed trend in vegetation phenology. Around 43% of the total global forest cover lost during 2000 to 2005 was from temperate and boreal regions (Hansen, Ruedy, Sato, et al., 2010; Hansen, Stehman, & Potapov, 2010). Hence, varying proportions of forest loss must exist in the GIMMS forest pixels, embedding a mixing effect in the NDVI signal that might potentially lead to false interpretation of the changes in SOS and EOS. Hence, data on global forest loss from 2000 to 2005 (Hansen, Ruedy, Sato, et al., 2010; Hansen, Stehman, & Potapov, 2010), provided by South Dakota State University (http://globalmonitoring.sdstate.edu/projects/gfm/global/gindex.html) were utilised to analyse this effect. The percentage forest loss was estimated within each GIMMS pixel. Temporal variation in the derived data (NDVI, SOS and EOS) was analysed within different percentage classes averaged above 45°N.

2.6. Vegetation type-wise analysis

The recently available MERIS Globcover 2009 (V2.3) data (300 m spatial resolution; http://ionia1.esrin.esa.int/) were used to identify different vegetation types. Of 23 classes available in the land cover map, eight vegetation classes (Classes 30 to 110) were used to cover the major woody vegetation types present above 45°N latitude. Vegetation classes covering smaller areas occurring above 45°N were not used. Although Classes 30, 110 and 130 to 180 are related to vegetation (see Table 2 for details), they are mainly mixed classes composing less woody forest and, hence, were not useful for this analysis. However, Classes 30 and 110 were considered to check the variability in SOS and EOS within the mixed classes. Classes 130 to 180 were not considered. The original Globcover data were rescaled (using majority aggregation) to match the exact pixel location of GIMMS and its spatial resolution. For each class the trends in SOS and EOS over the full 25 years were analysed.

For each vegetation class the percentage occurrence of that class within each GIMMS pixel was calculated. Then, 43 "core" areas were selected each occupying more than 80% by these vegetation classes and distributed above 45°N. These core zones provide controlled samples as they represent near homogeneous cover for a vegetation type and, thus, have a greater chance of showing the "real" trend in phenology for a specific vegetation type. Thus, the results from these sites should have greater reliability and can be used as a reference. In addition, the percentage vegetative cover image (8 km) was reclassified into 10 classes covering 10% each and then the mean SOS and EOS within these percentage classes were calculated for each class. In all the above analyses, a summary was made for all the pixels occurring above 45°N. The basic assumption was that a forest class with a high percentage canopy cover would be more likely to reveal a real change, if any, in phenology, relative to more mixed pixels.

3. Results

Two groups of latitudinal zones were created to investigate the temporal variation in NDVI and vegetation phenology: (a) 15°S–15°N, 15–45°N, >45°N, (b) 35–45°N, 45–55°N, 55–65°N, >65°N. However, the major analysis was carried out only over the zones 45–55°N, 55–65°N, >65°N and >45°N. The phenology parameters were also scrutinised within different vegetation types, core areas, percentage cover values and forest change values. The following sub-sections provide detailed results from these analyses, and the number of pixels used in the analysis was provided in Tables 1, 2, 3, 4, and Supplementary Tables S1 and S2.

3.1. Variation in NDVI

Fig. S1 (please see the supplementary data) shows 25 years of temporal variation in the NDVI time-series averaged (composite-wise mean) across three broad latitudinal zones (15°S–15°N; 15–45°N and >45°N). Fig. 3 shows yearly variation in NDVI during the peak period (i.e., seasonal amplitude; Jul–Aug average) which is useful in authenticating an increase or decrease in the intensity and spatial distribution of vegetation greenness. There was an observable increasing trend in the maximum amplitude during 1984 to 1990 (above 45°N zone) which matches observations by Myneni, Keeling, Tucker, et al. (1997), and a decreasing trend post-1997 which could be linked to forest cover loss as reported by Hansen, Stehman and Potapov (2010) or due to climatic factors. Piao, Wang, Ciais, et al. (2011) studied the variation in NDVI over the temperate and Boreal regions of Eurasia with respect to temperature and precipitation and revealed a decreasing NDVI pattern after 1997. The results from our study (Fig. 3) are in close harmony with their findings. They have attributed the decrease in NDVI to a remarkable decrease in summer precipitation in those regions.

Analysis of seasonal amplitude across five different latitudinal zones (35–45°N; 45–55°N, 55–65°N; >65°N and >45°N) revealed a consistent decreasing pattern after 1997 (Fig. 3). The spatial distribution of the percentage change in NDVI for the major growth phases; greening (Mar–Apr–May), peak growth (Jun–Jul–Aug) and senescence (Sep–Oct–Nov), and the corresponding statistically significant areas are given in Fig. 4. Most of the changes during the greening and senescing periods were positive (depicted by green to red colours in Fig. 4a, e). However, during the peak growth period the change in NDVI was mainly negative (depicted by bluish tones in Fig. 4c), except for a few highly clustered patches of positive increase in North America, which explains the decrease in seasonal amplitude. It was found that, during the peak growth period, an area of 6.5 million km^{-2} exhibited a 20% decrease in NDVI (spread across northern latitude), whereas an area of 4.7 million km^{-2} exhibited a 20% increase in NDVI (mainly in North America and Eastern Europe). Statistically significant changes (95% confidence level) during the greening period were clustered mainly in Europe, but for the peak growth period were clustered around north-western America, and for the senescence period were distributed over northern USA and Eastern Europe.

Since each composite was analysed separately over 25 years, the number and distribution of pixels obeying the initial reliability conditions were different in each composite (this difference can be seen between Fig. 4a, c, e; see Section 2.1 for clarity).

3.2. Latitudinal variation in SOS and EOS

The start of season (SOS) and end of season (EOS) were estimated for each available high quality pixel. When the SOS and EOS results were averaged for all high quality pixels above 45°N (Fig. 5a, c), it revealed a weak trend towards early SOS with a rate of change of -0.13 days yr^{-1} ($r^2 = 0.21$) and similarly a weak trend towards delayed EOS with a rate of change of $+0.17$ days yr^{-1} ($r^2 = 0.19$) (both trends were significant with $p < 0.05$). Table 1 provides a summary and comparison of the statistical trends in SOS and EOS for different latitudinal zones. The results reveal that the changing trend in EOS is faster than for SOS.

Further analysis at three sub-latitudinal zones (Fig. 6a, c), for SOS, revealed no statistically significant trend over the 45 to 55°N ($r^2 = 0.094$) and above 65°N zones ($r^2 = 0.089$), and a weak, but significant ($p < 0.05$) trend with a rate of change of -0.19 days yr^{-1} for the 55 to 65°N zone ($r^2 = 0.18$). For EOS, weak, but statistically significant ($p < 0.05$) trends were found for the 45 to 55°N zone ($r^2 = 0.24$; $+0.19$days yr^{-1}) and the 55 to 65°N zone ($r^2 = 0.16$; $+0.20$ days yr^{-1}), but no significant trend for the above 65°N zone ($r^2 = 0.0006$).

Fig. 7a, c illustrates the spatial distribution in the rate of change in SOS and EOS (in days yr^{-1}), respectively, while Fig. 7b, d illustrates the spatial distribution of statistically significant areas. It was found that the trend from 1982 to 2006 was statistically significant for around 10% of all pixels, for both SOS and EOS, and the reliability of these pixels is expected to be high. White, deBeurs, Didan, et al. (2009) also revealed, in their study of spring phenology in North America during 1982–2006, that only 12% of the area showed a statistically significant trend in SOS. Hence, further analysis focusing on the variability in SOS and EOS within only these significant pixels (i.e., using this condition as a mask) was carried out for the >45°N zone (Fig. 5b, d) and for other latitudinal zones (Fig. 6b, d). The trend became nearly four times stronger ($p < 0.01$) than when considering all high quality pixels. Considering only statistically significant pixels results in a 14.5 days (-0.58 $daysyr^{-1}$) advancement in SOS and 16 days ($+0.64$ days yr^{-1}) delay in EOS over 25 years. These results are comparable with ground-based studies (Fitter & Fitter, 2002; Menzel & Fabian, 1999; Stockli & Vidale, 2004).

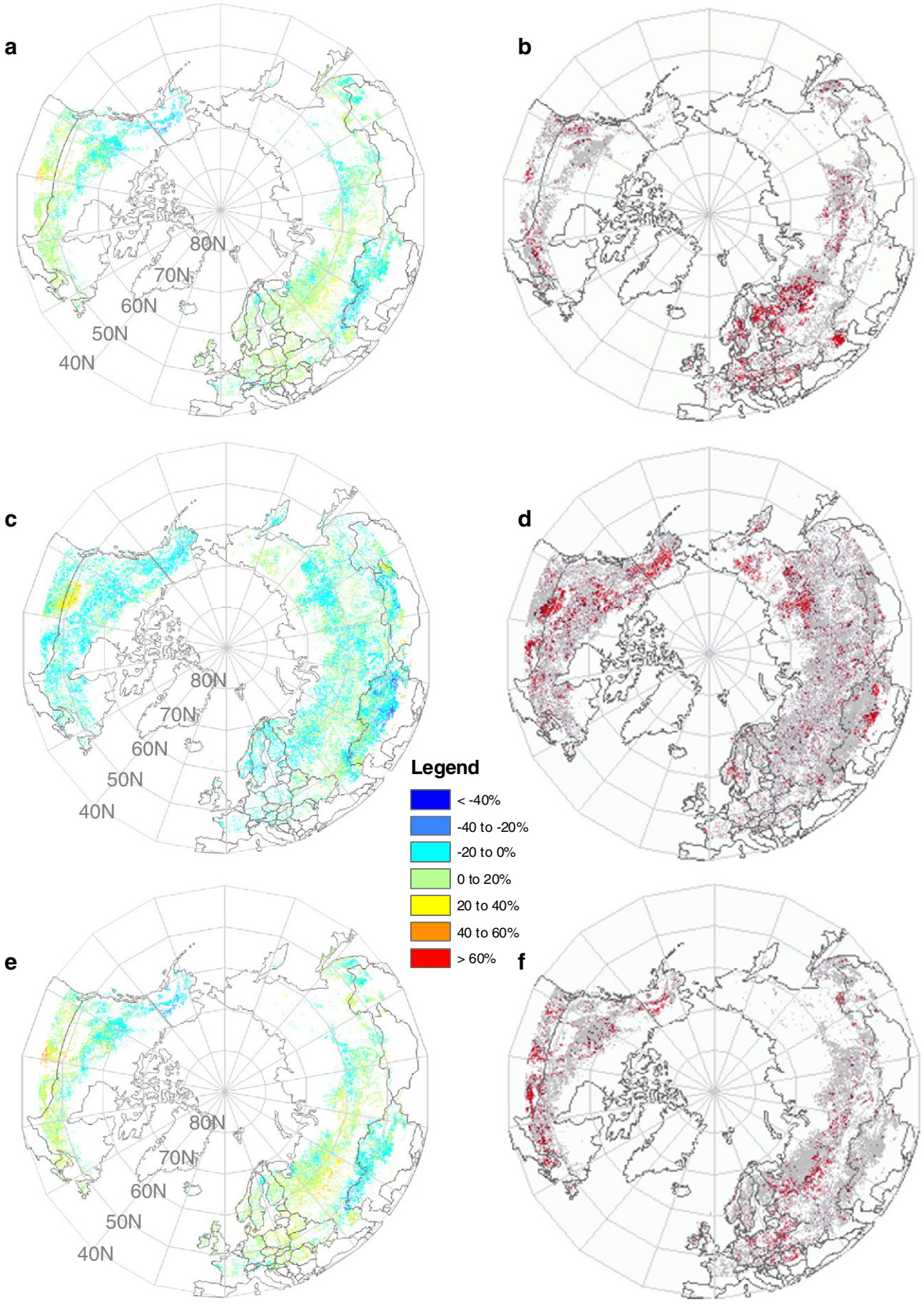
a
b
c
d
e
f
80N
70N
60N
50N
40N
Legend
< -40%
-40 to -20%
-20 to 0%
0 to 20%
20 to 40%
40 to 60%
> 60%

3.3. Variation in phenology within different proportions of forest loss

Data on global forest loss during 2000 to 2005 (Hansen, Ruedy, Sato, et al., 2010; Hansen, Stehman, & Potapov, 2010) were upscaled to estimate the proportions of loss within each GIMMS pixel and, subsequently, to investigate the variation in SOS and EOS within different forest loss scenarios. It was noticed that the majority of the forest loss was spread across Russia and North America. The resultant trends in SOS and EOS within different proportions of forest loss are provided in Table S1. Fig. 8a, c show the mean temporal variation, averaged above 45°N, in SOS and EOS for high quality pixels subject to different proportions of forest loss. Using only significant pixels, the variation in SOS and EOS is depicted in Fig. 8b, d. There is a clear dip in SOS in the year 1998 (Fig. 8a, b) indicating a very early SOS in the areas subject to forest loss. Large scale climatic variability like El Nino and small scale microclimate fluctuations affect plant phenology (Asner, Townsend, & Braswel, 2000; Jackson, 1966). Interestingly, 1997–98 was an El Nino year and it was the strongest on record (McPhaden, 1999) and our results suggest its potential effect on advancement in SOS. Its impact varies with different vegetation types and regions, being greatest for vegetation located on the western coast of North America. However, detailed influence of El Nino on the phenology of vegetation at higher latitudinal zones was not the focus of this research as it requires further investigation. For the areas subject to small proportions of forest loss (<20%) there is no trend in SOS, but there is a significant mean delay of $+0.71$ days yr^{-1} in EOS. In fact, no trend was expected when more than 80% of the forest was lost, but the results revealed an increasingly early SOS for areas subject to more than 60% forest loss. This might be due to NDVI values from early growing grass and shrubs in the cleared regions with early snow melt (Stockli & Vidale, 2004).

3.4. Variation in phenology within specific vegetation types

The phenology results from 1982 to 2006 were tested statistically within several vegetation classes (see Table 2). It was found that, when all high quality pixels were used, only the Class 100: Closed to open (>15%) mixed broadleaved and needle leaved forest (>5 m) yielded a significant trend for both SOS and EOS. Classes 50: Closed (>40%) broadleaved deciduous forest (>5 m) and 70: Closed (>40%) needle leaved evergreen forest (>5 m) did not show any significant trend for SOS but the trend was significant for EOS. Class 90: Open (15–40%) needle leaved deciduous or evergreen forest (>5 m) did not reveal a trend for both SOS and EOS when all high quality pixels were considered.

It may be possible that the spatial distribution of diverse vegetation types across different environmental conditions contributed towards averaging out locally significant trends. Hence, the analysis was repeated by vegetation type using both high quality and significant pixels separately and Figs. 9 and 10 present the variation in the SOS and EOS, averaged over the '>45°N' zone, respectively. It was observed that the inter-annual fluctuation in SOS was greater than for EOS (Fig. S2).

From the classes considered, Classes 90 and 100 exhibited a higher rate of change for both SOS (-0.73, -0.66) and EOS ($+0.60$, $+1.01$) (Table 2, Fig. 9) than the other classes. Interestingly, the needle leaved vegetation in the Globcover 2009 data is a mix of both deciduous and evergreen types, and hence it was not possible to differentiate the nature of the trends in SOS and EOS for these two completely different groups. Also, there is already a separate class for *needle leaved evergreen forest* (Class 70) and hence Class 90 could be considered as a representative for *needle leaved deciduous forest*.

The reliable, homogeneous classes of broad leaved (deciduous) and needle leaved (evergreen) forest (Classes 50 and 70) showed the least advancement (-0.27 and -0.25 days yr^{-1}, respectively) in SOS compared to the other classes, but a significant delay in EOS after 1993 (Fig. 9).

Further analysis was undertaken to extract the trends in SOS and EOS for vegetative classes within different latitudinal zones using significant pixels alone (Figs. S3 and S4). It was observed that Class 50 showed consistent and significant trends in SOS and EOS for all latitudinal zones. Class 90 also showed significant trends, but not for SOS at 45–55°N. Table 3 reveals the actual trend values, statistical significance and correlation coefficients for SOS and EOS for all classes and for all latitudinal zones. The longest delay in EOS was observed for Class 50 in the 55–65°N latitude zone ($+1.22$ days yr^{-1}). For SOS, the latitude zone 55–65°N showed the overall largest trend (mean of -0.71 days yr^{-1}). The latitude zone 45–55°N showed the overall largest EOS trend (mean of $+0.88$ days yr^{-1}). Since the number and distribution of significant pixels were different for SOS and EOS (as the model fitting processes were independent for these two variables), some classes have fewer or no pixels in some latitudinal zones and, hence, the trend values were either not available or not significant in Table 3.

3.5. Variation in phenology within "core" areas of vegetation

All the analysis and results presented above reflect the latitudinal average (>45°N). Thus, the effects of local scale environmental factors on phenology have been masked. Hence, 43 relatively small, but highly homogeneous (>80% cover) core areas of different vegetation classes (Fig. S5) were selected for investigation. Temporal variation in the 25 years of mean NDVI within these core areas was analysed. Core areas from two different regions are presented for each class revealing the actual variation and complexity. The SOS and EOS estimated for these core areas are presented in Fig. 10 for Classes 30 and 50 and in Fig. 11 for Classes 70 and 90.

The trends in SOS and EOS were not smooth as expected, but highly fluctuating in these core areas which might be mainly due to local climatic variability. Class 30 did not reveal any trend for SOS, but the core area from North America revealed a positive trend for EOS (i.e., delayed EOS) and the European core area revealed a negative trend (i.e., earlier EOS). Similarly, Class 50 did not show any trend for SOS, but weak trends of increasing delay in EOS were found for both the core areas from Russia and North America. Class 70 from North America revealed a pronounced delay in EOS after 1996, and no trend for SOS. For Class 90, the core area from North America revealed a mean trend as a curvy pattern with early SOS during the 1980s and delayed SOS after 1998, and increasingly delayed trends in SOS and EOS were found for the core area from Russia.

3.6. Variation in phenology within areas with different proportions of vegetation

The average trend in phenology for each vegetation class as estimated above is bound to have some uncertainty because GIMMS pixels at 8 km spatial resolution contain different proportions of the vegetation classes. Hence, the variation in the trends for different proportions of each class was investigated to provide useful information for ground-based studies. Furthermore, the higher proportion categories should cover the "core" areas in each class as defined above and, hence, should provide reliable estimates of trends.

The spatial distribution of the estimated percentages of the vegetation classes occurring within the GIMMS pixels is given in

Fig. 4. Spatial distribution of percentage change in mean NDVI (1982–2006) during (a) Mar–Apr–May (c) Jun–Jul–Aug and (e) Sep–Oct–Nov. The corresponding 95% significant pixels are shown in (b), (d) and (f) (red indicates significant areas).

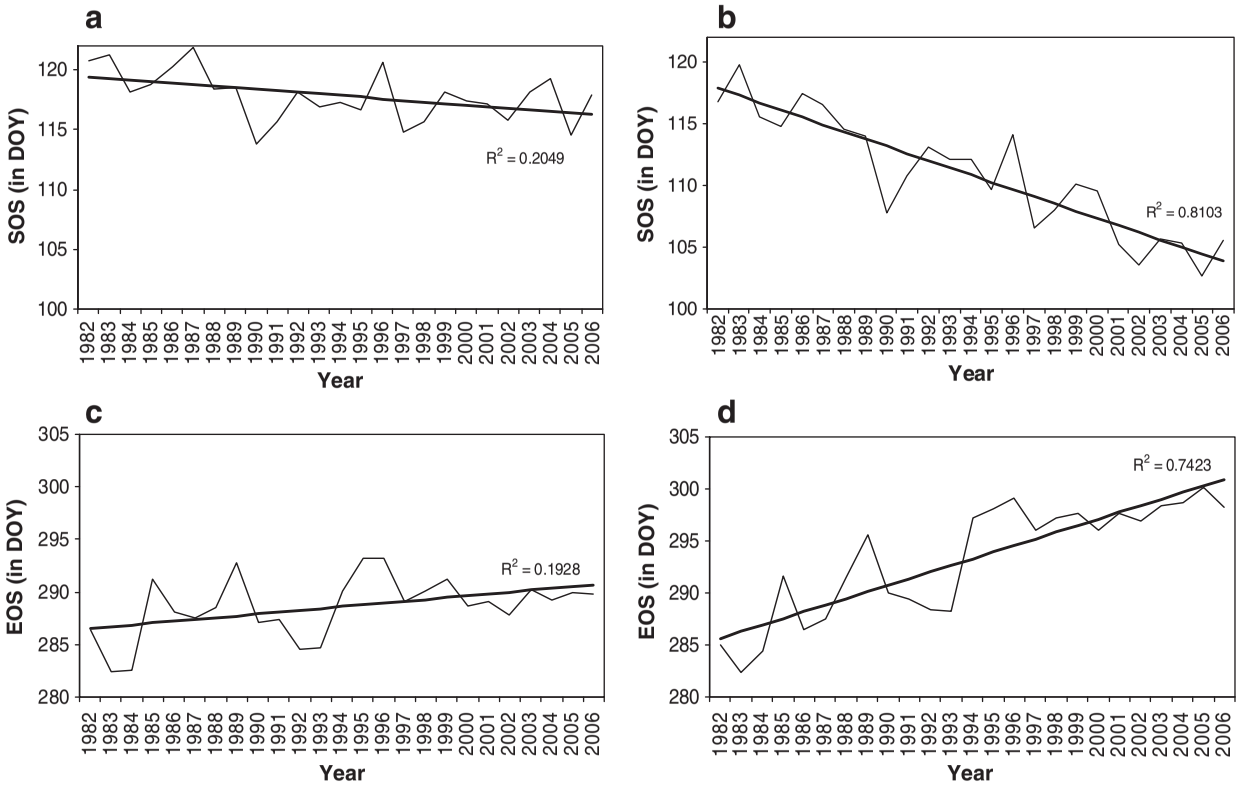

Fig. 5. Long-term variation in date of (a) SOS and (c) EOS during 1982–2006 over northern latitudes (above 45°N) and results for (b) SOS and (d) EOS using significant pixels alone.

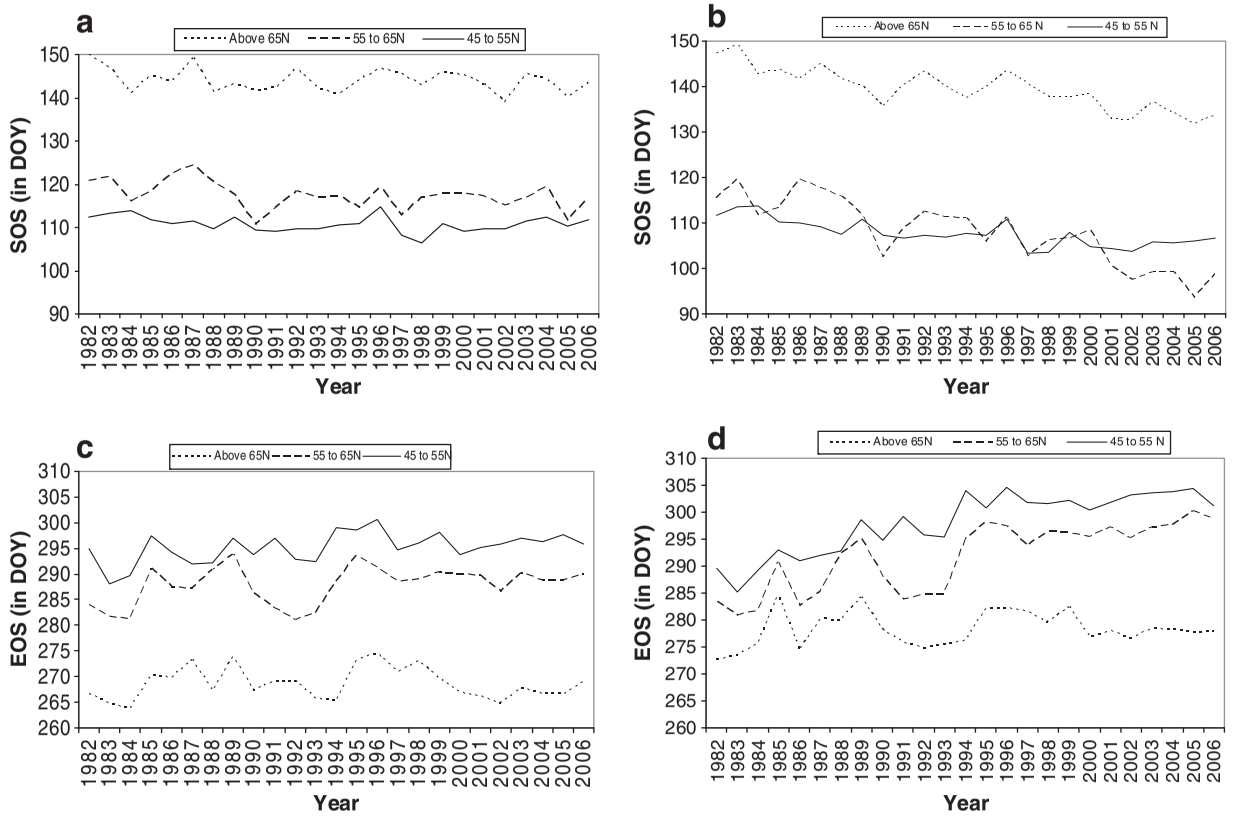

Fig. 6. Long-term variation in date of (a) SOS and (c) EOS during 1982–2006 at different latitudinal zones, and results of (b) SOS and (d) EOS using significant pixels alone.

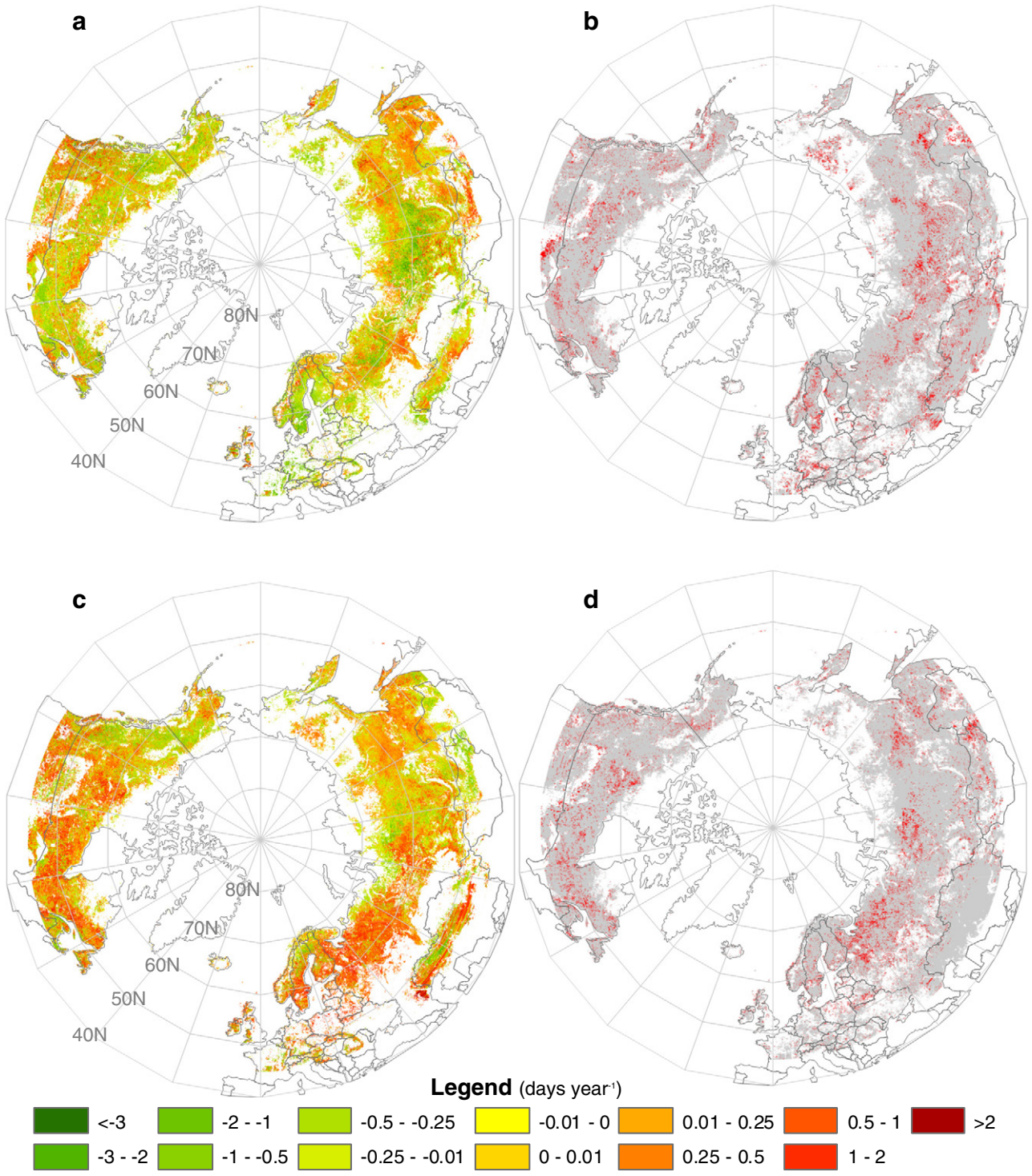

Fig. 7. Spatial distribution of rate of change in (a) SOS and (c) EOS during 1982–2006 and pixels for which rate of change is statistically significant at 95% confidence level for (b) SOS and (d) EOS (red colour indicates statistically significant areas).

Fig. S6. Although the number of higher proportion pixels is small for most classes, it is sufficient to reveal the trend in SOS and EOS. Moreover, these 8 km pixels were derived through aggregation from the 300 m spatial resolution Globcover data and, hence, were highly reliable. From all classes, Class 90 covers the largest area (i.e., 7% of the total area) and also has more pixels with higher percentage (71 to 100%) cover. Thus, results are expected to be more reliable for this class.

The variation in mean SOS and EOS within different ranges of percentage cover for each vegetation class was estimated within the '>45°N' zone. Figs. S7, S8, 12 and 13 provide a graphical depiction of the variation in SOS and EOS for only the higher percentage categories (>50% proportions) in each of the classes. Table S2 reveals the statistical significance and correlation coefficient for each proportion range under each vegetative class. For the Mosaic vegetation class, Open needle leaved deciduous or evergreen forest and Closed to open mixed broad

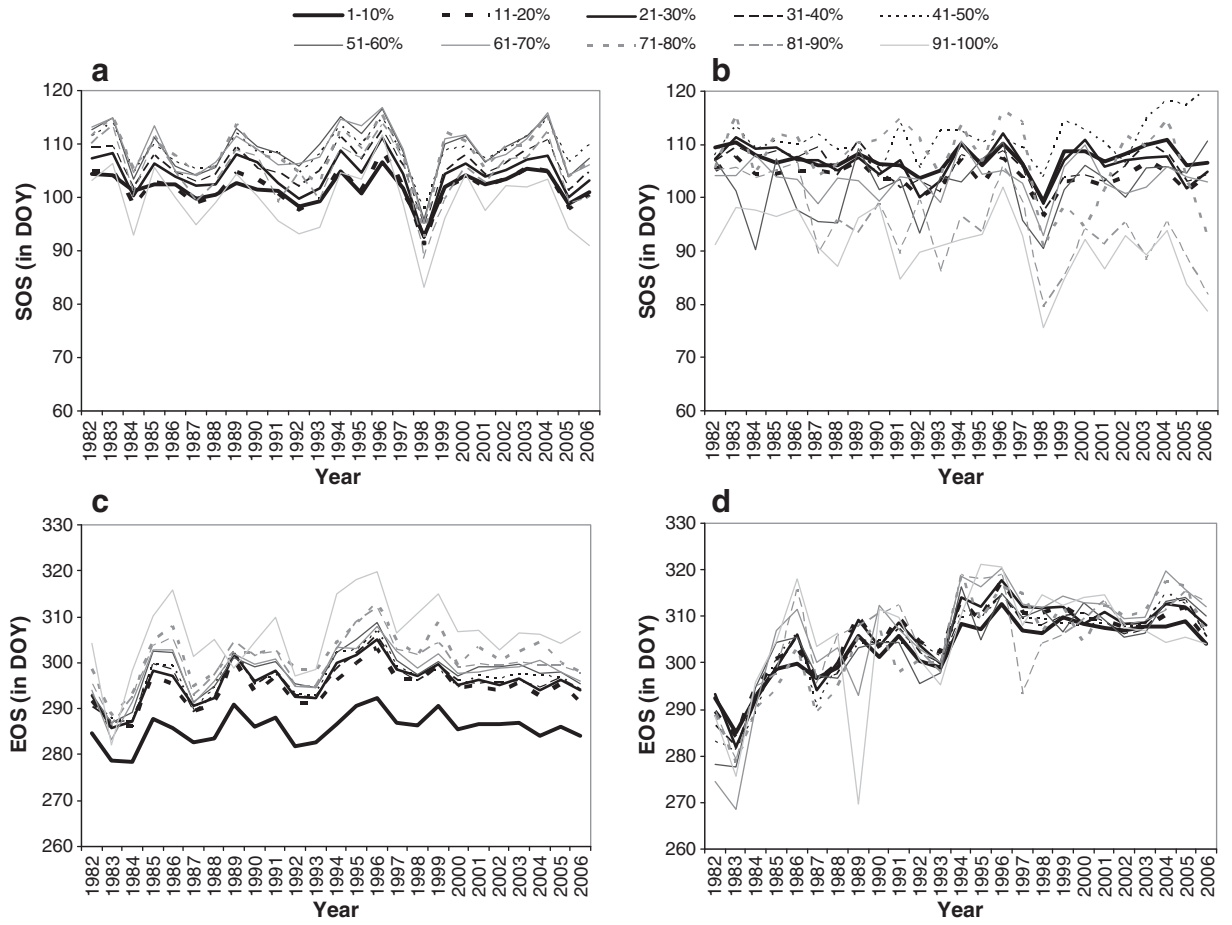

Fig. 8. Trends in (a) SOS and (c) EOS within areas of different percentages of forest loss (above 45°N), and the results (b) SOS and (d) EOS after using significant pixels alone.

leaved and needle leaved forest SOS became significantly earlier (Fig. 12a, c, e).

The rate of change in SOS and EOS was analysed within different proportions of each vegetation type, and the results from the '>45°N' zone using all high quality pixels are presented in Fig. S9a, c while the results using only significant pixels are shown in Fig. S9b, d. The analysis using significant pixels revealed that on average the SOS moved earlier by -0.40 days yr^{-1} and EOS delayed by $+0.65$ days yr^{-1}, when all proportions from Classes 30, 50, 70, 90 and 100 are considered. But, the slope of the trend is less steep with -0.21 days yr^{-1} for SOS and $+0.5$ days yr^{-1} for EOS when only the vegetation proportions above 70% are considered. In both cases, the delay in EOS is consistently larger than the advancement in SOS, which leads to the inference that autumnal response of vegetation is greater and faster than that in spring.

When individual classes are analysed for vegetation proportions over 70%, considering the '>45°N' zone, the SOS trend was -0.15, $+0.00$, $+0.02$, -0.16, -0.11, and $+0.16$ days yr^{-1} and the EOS trend was -0.04, $+0.22$, $+0.39$, $+0.14$, $+0.16$, and $+0.20$ days yr^{-1} for the Classes 30, 50, 70, 90, 100 and 110, respectively. When only the significant pixels were considered, for >70% proportions, the SOS trend was -0.58, $+0.08$, -0.10, -0.80, -0.52, and $+0.45$ days yr^{-1} and the EOS trend was -0.39, $+0.58$, $+1.22$, $+0.52$, $+0.50$, and $+0.84$ days yr^{-1} for the Classes 30, 50, 70, 90, 100 and 110, respectively.

Finally, the significant pixels in the highest proportion class (covering 91 to 100% tree cover) amongst each vegetative class were analysed for different latitudinal zones (Table 4). This analysis revealed once again that the change in phenology trend was faster and larger in the 55–65°N zone, as observed in the previous sections. The largest advancement in SOS (-1.07 days yr^{-1}) was found for the *needle leaved deciduous vegetation* (Class 90) within the 55–65°N zone. The largest delay in SOS ($+1.06$ days yr^{-1}) was observed for the *broad leaved deciduous vegetation* (Class 50) within the 55–65°N zone. Interestingly, the Classes 50, 70 and 90 revealed a delay in SOS within the 45–55°N zone. Deciduous broad leaved vegetation revealed a shrinking growth cycle with delayed SOS and earlier EOS within the 45–55°N zone. This requires detailed ground evaluation. Classes 70 and 90 exhibited delays in both SOS and EOS within the 45–55°N zone, which resembles a backward translation in growth cycle. Class 100 revealed an advancement in both SOS and EOS within the >65°N zone, which resembles a forward translation in growth cycle.

4. Discussion

Field based observations and studies as reported in the literature have revealed a clear temporal shifting in the phenological rhythm of plants. Although they all agree on a lengthening of the growing season, their individual findings are different mainly due to the differences in the scale, vegetation type, composition and other environmental factors in those studies. On a hemispherical scale, satellite-based studies have been demonstrated to be useful. However, there is much uncertainty in the results when representing changes in vegetation phenology as latitudinal averages due to the integration within pixels of different environmental and vegetative conditions. In response to concerns over the validity of satellite-based studies of phenology, the current research adopted a strict approach to the selection of pixels for analysis through statistical tests of significance at different levels and through various stratification schemes. The current research revealed varying amounts of uncertainty associated with the detected values of, and trends in, SOS and EOS from 1982 to 2006. It is important to note here that when the spatio-temporal variation in the onset of snowmelt

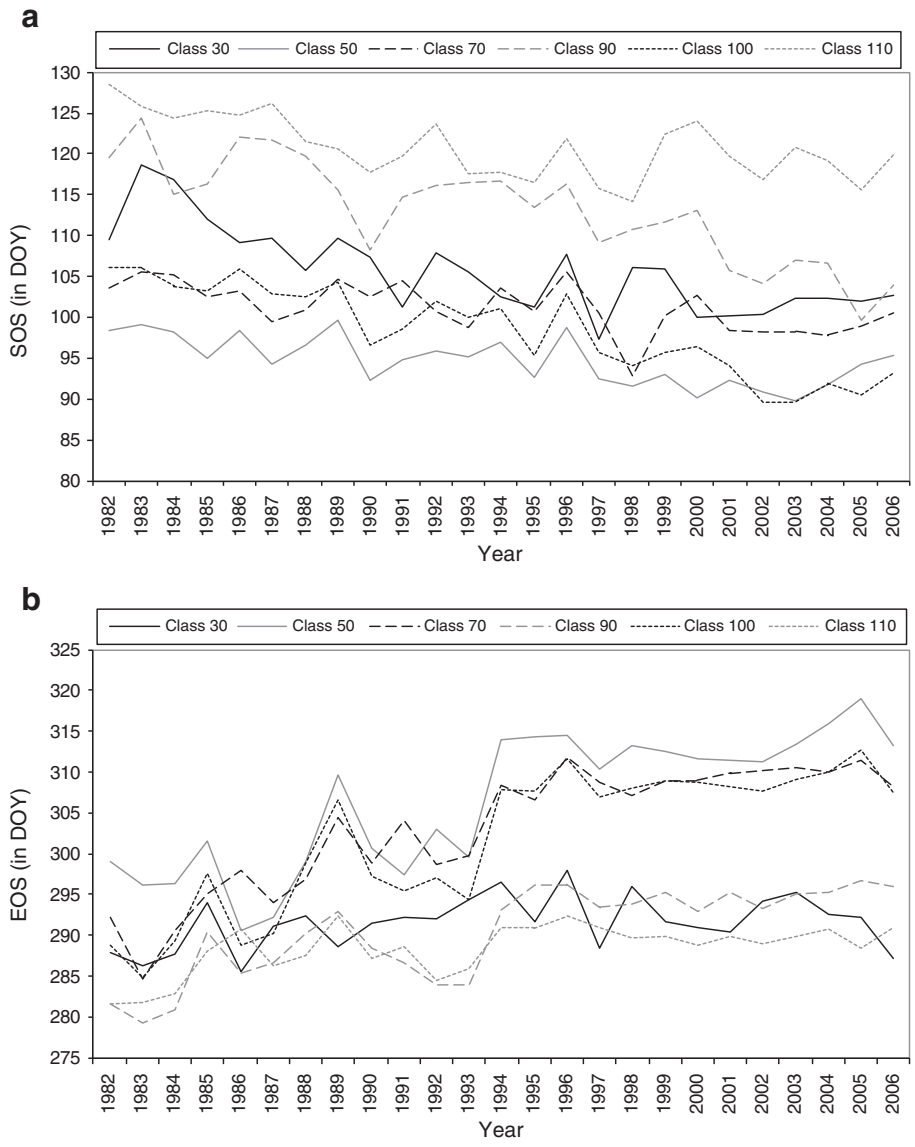

Fig. 9. Variation (>45°N) in the (a) SOS and (b) EOS during 1982–2006 by vegetation class using significant pixels alone.

due to a changing climate is not uniform across different regions (Anderson & Drobot, 2001), we may also expect the same for vegetation as both processes are influenced by temperature.

Wang et al. (2011) studied the variation in NDVI with reference to temperature in North America, and revealed a temporal flip in the NDVI trend at different locations matched to temperature tipping points. This research provides information on the long-term trend in the 'above 45°N' zone, which agrees with Wang et al. (2011) over North America. Mao, Xiaoying, Peter, et al. (2012) examined the causative factors behind the NDVI changes during spring in mid-high latitudes (>25°N) and revealed that temperature is the primary causative factor in explaining variation in NDVI in relation to turning point trends.

SOS and EOS over 25 years revealed a non-uniform pattern with much fluctuation, and this inter-annual variability has a potential link with the global circulation pattern. For example, Hurrell and van Loon (1997) studied 130 years of variability in the North Atlantic Oscillation (NAO) and revealed an extreme phase of NAO since 1980 which resulted in surface warming over Europe during the winter and a cooling effect in the northwest Atlantic. Stockli and Vidale (2004) also revealed a correlation between springtime NDVI and wintertime NAO index anomalies. Menzel, Sparks, Estrella, et al. (2005) and Gouveia, Trigo, DaCamara, et al. (2008) found a link between NAO and changes in vegetation growth patterns in Europe.

The SOS and EOS trends derived in this research (Figs. 6 and 7; Section 3.2) are comparable to results from previous ground studies. For example, Fitter and Fitter (2002) revealed a 4.5 to 15 days per decade advancement in the flowering time of plants in Britain. While Stockli and Vidale (2004) revealed a -0.54 days yr^{-1} advancement in SOS for European plants (1982 to 2001). Menzel and Fabian (1999) revealed an extended growing period in Europe with 6.3 day advancement in SOS and 4.5 day delay in EOS during 1951 to 1996. The observed changes in vegetation phenology seem to be smaller when compared to climate change impacts on snow and lake ice phenology. For example, Rotschky, Schuler, Haarpaintner, et al. (2011) studied the spatio-temporal variability of snow melt in Norway during 2000 to 2009 and revealed around a 10 day advancement (-1.0 days yr^{-1}) in the onset of snowmelt. Latifovic and Pouliot (2007) revealed an earlier (-0.99 days yr^{-1}) break-up in lake ice and delayed freezing ($+0.76$ days yr^{-1}) in Canada during 1985–2005.

An important finding in this research is that the changing trend in EOS is faster than that in SOS, and the same has been observed in ground

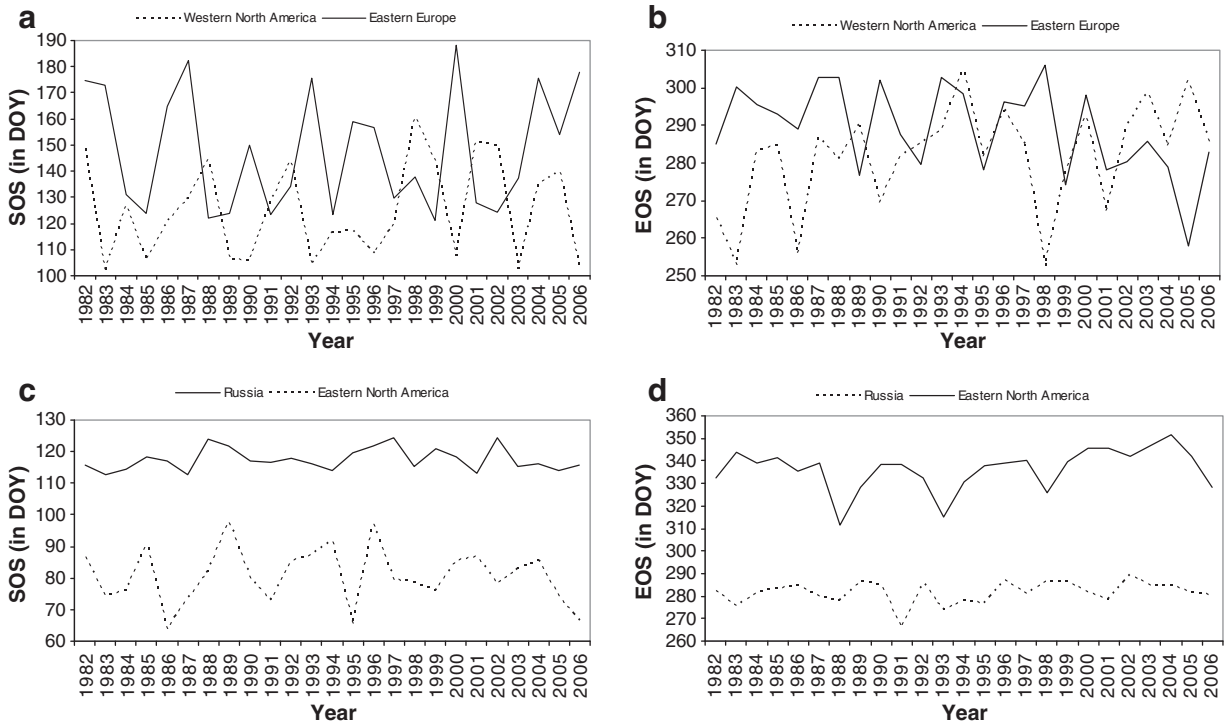

Fig. 10. Temporal variation in SOS within core areas of (a) Class 30 and (c) Class 50 and temporal variation in EOS within core areas of (b) Class 30 and (d) Class 50.

studies. For example, Karlsen, Hogda, Wielgolaski, et al. (2009) revealed a larger and faster trend for EOS (+0.37 days yr^{-1}) than SOS (−0.27 days yr^{-1}) in the Fennoscandia region during 1982–2006. The zone 55 to 65°N seems to be a sensitive zone because both the SOS (−0.86 days yr^{-1}) and EOS (+0.71 days yr^{-1}) trends were larger here than for all other zones (Table 1). The effect of changing climatic condition is thought to be larger here as it is a convergence zone for the Arctic and Atlantic oceanic circulation. These shifts in phenological variables are conceptualised to affect the vegetation-atmospheric feedback (Richardson, Anderson, Arain, et al., 2012). However, separating

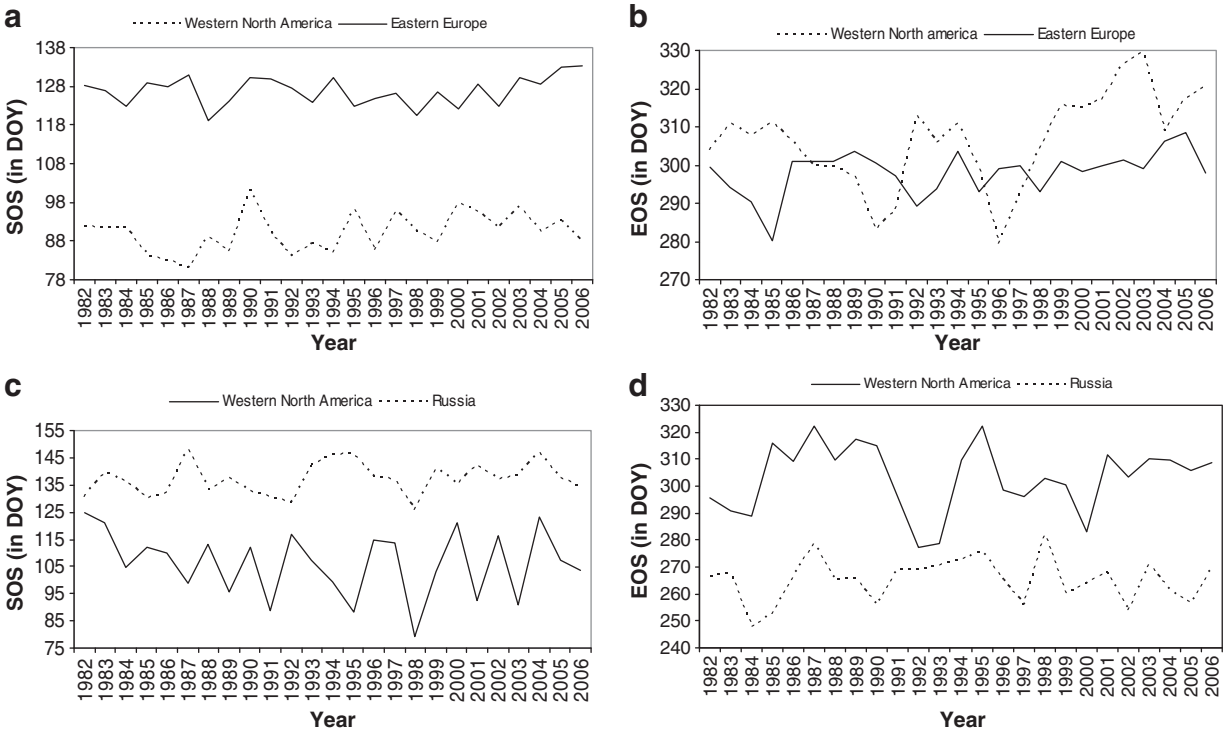

Fig. 11. Temporal variation in SOS within core areas of (a) Class 70 and (c) Class 90 and temporal variation in EOS within core areas of (b) Class 70 and (d) Class 90.

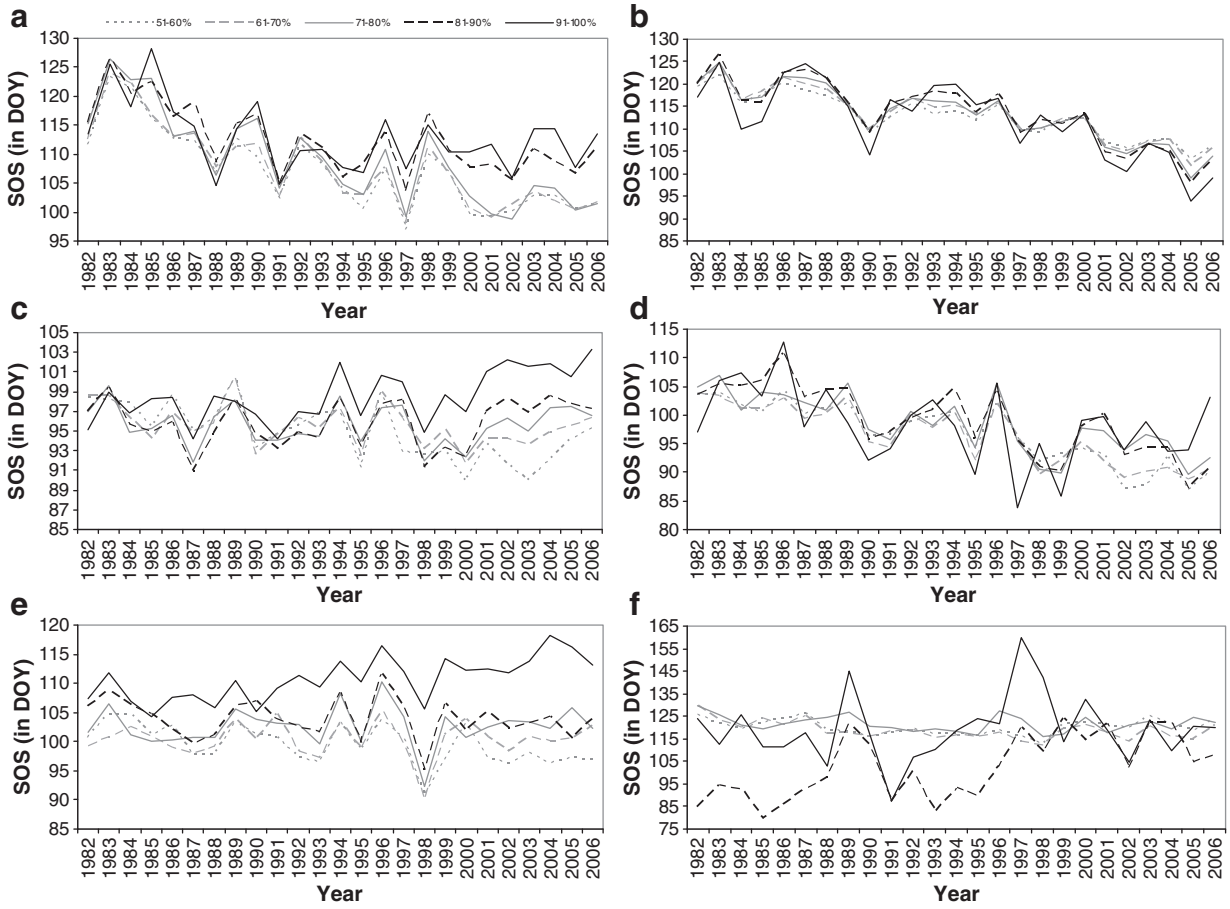

Fig. 12. Percentage-wise variation in SOS within different vegetation classes occurring >45°N using only significant pixels: (a) Class 30; (c) Class 50; (e) Class 70; (b) Class 90; (d) Class 100 and (f) Class 110.

these changes at key phenological stages is important as the environmental variables controlling vegetation photosynthesis have varied effects depending on the phenological stages and, in turn, atmospheric feedbacks. For example, temperature may be the controlling factor for photosynthesis during spring (Menzel, Sparks, Estrella, et al., 2006) whereas the photoperiod has been shown to have more control on autumn productivity of vegetation (Bauerle, Oren, Way, et al., 2012). Therefore, the climate carbon models used to predict the impact of climate change on the terrestrial biogeochemical cycle (Knorr, Kaminski, Scholze, et al., 2010; Randerson, Hoffman, Thornton, et al., 2009) should consider a variable rate of changes in the SOS and EOS.

It was argued that an increase (decrease) in NDVI in the spring (autumn) could be due to an earlier (delayed) snowmelt (Stockli & Vidale, 2004). We found some link between the trend in the onset of snowmelt and inter-annual variation in SOS and EOS, although detailed analysis was not the focus of this study. Drobot and Anderson (1999) estimated the date of onset of snowmelt at different locations across the Arctic sea ice between 1982 and 1992. From their research it was noticed that 1990 was the year of early snowmelt with 15 days advancement compared to other years and this could be linked to a dip (i.e., advancement of around 10 days in a single year) in SOS for the year 1990 (Figs. 5, 6a, b).

Interestingly, the pixels in the 91–100% proportion from broadleaved deciduous vegetation (Class 50) (Fig. 12c) revealed a statistically significant ($p < 0.01$) trend of delayed SOS ($+0.22$ days yr^{-1}), and the delay was mainly after 1998. Wang, Piao, & Ciais, et al. (2011) revealed that the spring temperature change in North America was not uniform and there were patches after 1996 exhibiting tipping points (high to low and *vice versa*) in temperature. It may be possible that such a temperature reversal had a cooling effect, delaying the SOS in the dense patches (>50% categories) of the broadleaved deciduous vegetation type (Class 50). Kross, Fernandes, Seaquist, et al. (2011) also observed a delay in the SOS with trends varying from $+0.02$ to $+0.26$ days yr^{-1} over 23 years (1985–2007) for the broadleaf forests in the majority of ecozones (Mixed woodplains, Boreal shield, Boreal Plains, Atlantic maritime and Prairies) in Canada, and for some zones (Taiga plains, Pacific maritime and Montane cordillera) it varied from -0.03 to -0.44 days yr^{-1}. A similar delayed trend in SOS was seen only for very dense (91–100% category) *needle leaved evergreen vegetation* (Class 70), and for other ranges of proportions there was a weak-to-no-trend. Most of the classes revealed a statistically significant delayed trend for EOS (Fig. 13), except Class 30 (Table S2). All the higher proportions categories in Class 90 revealed a consistently significant early trend for SOS (Fig. 12b) and consistent delaying trend for EOS (Fig. 13b). For the Classes 50, 70 and 90, the year 1993 seems to be a tipping year as the delay in EOS trend became more pronounced. It was observed that for some of the higher proportion categories there was no significant trend (especially Class 70 for SOS) which may be due to the smaller number of pixels available or due to the mixing of patterns from pixels with different environmental conditions.

The majority of the high proportion pixels from Class 90 are located in Russia, dominated by larch forest (*Larix*) (Stolbovoi, 2006; see Fig. 1a, page 206). Stolbovoi (1999) classified Russian forests in relation to climatic warming based on the thermal characteristics of forests and

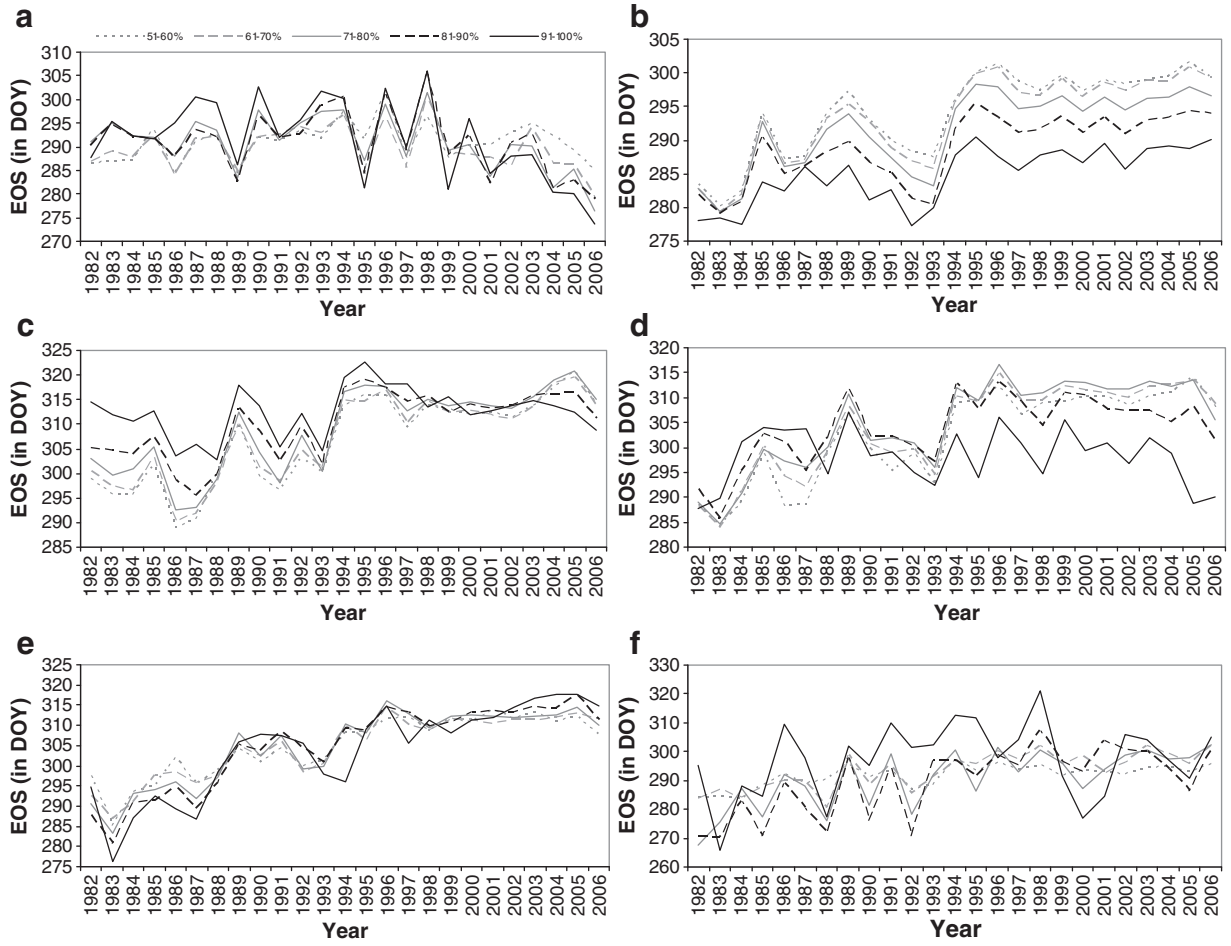

Fig. 13. Percentage-wise variation in EOS within different vegetation classes occurring >45°N using only significant pixels: (a) Class 30; (c) Class 50; (e) Class 70; (b) Class 90; (d) Class 100 and (f) Class 110.

provided a link between the frequency of forest appearance as a function of mean annual temperature. A recent study by Zhang, Yasunari, and Ohta (2011) revealed that under a future global warming scenario (+2 °C or higher) the forest–permafrost coupled system would be altered drastically which would lead to extinction of larch. In the current study, Class 90 exhibited a consistently significant trend in SOS and EOS, and it is the only class which showed a declining trend in SOS (15 to 21 days over 25 years) greater than the increasing trend in EOS (11 to 18 days over 25 years). This may reflect a faster adaptation strategy of the plant for its regrowth. However, how far such advancement can move is debatable.

Although the Globcover2009 data has a very fine spatial resolution (300 m), its class definitions are very coarse with many mixed classes. This posed a difficulty in explaining unexpected temporal patterns in SOS and EOS in some of the mixed classes.

5. Conclusion

Considering the importance of quantifying long-term changes in the carbon cycle and its associated link with the vegetation growth cycle, the current research attempted to reduce the uncertainty in the previously estimated SOS and EOS trends by analysing long-term satellite-derived NDVI at different measurement levels, controlling for the effects of land cover change and vegetation type. The results can be summarised as follows.

In the '>45°N' zone, there was an advancement of 14.5 days in SOS and a delay of 16 days in EOS. When the amount of forest loss was incorporated, there was no trend for SOS within the near-intact areas (less than 10% forest loss), but a significant delay in EOS of 17.25 days over 25 years. In areas where more than 50% of the forest was lost, there was a mean advancement of 7 days in SOS and a delay of 21 days in EOS over 25 years.

It was thought that the background signal due to early growth of grass or shrubs could have altered the NDVI signal and, hence, might have contributed to a false early growth. However, further scrutiny of different vegetative classes revealed a clear shift in SOS and EOS for some classes. A few classes only showed clear patterns of change; *Needle leaved deciduous vegetation* (Class 90) (−18.25 days in SOS; +15 days in EOS) and *Closed to open mixed broad leaved and needle leaved forest* (Class 100) (−16.5 days in SOS; +25.25 days in EOS), when only significant pixels were considered (see Table 2 for details). The latitudinal zone covering 55–65°N exhibited the fastest trend in SOS (17.75 days advancement) while for EOS the fastest trend (30.5 day delay) was found in the 45–55°N zone. *Needle leaved deciduous vegetation* (Class 90) revealed the maximum advancement in SOS (25.75 days) within the 55–65°N zone, and *broad leaved deciduous vegetation* (Class 50) revealed the maximum delay (30.5 days) for EOS within the 55–65°N zone (see Table 3 for details).

Importantly, when data on vegetative proportional cover were considered, restricting the analysis to pixels with the larger proportions (>50%), a shifting trend (i.e., early SOS and delayed EOS) was observed

only for *needle leaved deciduous vegetation* (Class 90) (−18.55 days in SOS; +14.95 days in EOS on an average) and *mixed broad leaved and needle leaved forest* (Class 100) (−14.15 days of advancement in SOS and +18.05 days of delay in EOS on an average over the 25 years). For other classes a clear trend was found mainly for EOS, reflecting a delayed EOS (see Table S2 for details). For near-homogeneous vegetated areas (91–100% cover) the maximum advancement in SOS was 26.75 days for needle leaved deciduous vegetation within the 55–65°N zone, and maximum delay in EOS was 26.5 days for broad leaved deciduous vegetation within the 55–65°N zone (see Table 4 for details).

Acknowledgements

The authors wish to thank Geography and Environment, University of Southampton for providing a Fellowship to CJ during the study. Thanks are due to the NASA and GIMMS teams for making the 25 years of processed AVHRR NDVI data freely available to researchers. Thanks are also due to all the anonymous reviewers for their constructive and critical comments which helped to improve the quality of the paper.

Appendix A. Supplementary data

Supplementary data to this article can be found online at http://dx.doi.org/10.1016/j.rse.2013.11.020.

References

Anderson, M. R., & Drobot, S. D. (2001). Spatial and temporal variability in snowmelt onset over Arctic Sea ice. *Annals of Glaciology*, *33*, 74–78.
Asner, G. P., Townsend, A.R., & Braswel, B. H. (2000). Satellite observation of El Niño effects on Amazon Forest phenology and productivity. *Geophysical Research Letters*, *27*(7), 981–984.
Atkinson, P.M., Jeganathan, C., Dash, J., & Atzberger, C. (2012). Inter-comparison of four models for smoothing satellite sensor time-series data to estimate vegetation phenology. *Remote Sensing of Environment*, *123*, 400–417.
Bauerle, W. L., Oren, R., Way, D. A., Qian, S. S., Stoy, P. C., Thornton, P. E., et al. (2012). Photoperiodic regulation of the seasonal pattern of photosynthetic capacity and the implications for carbon cycling. *Proceedings of the National Academy of Sciences*, *109*(22), 8612–8617.
Bradshaw, C. J. A., Warkentin, I. G., & Sodhi, N. S. (2009). Urgent preservation of boreal carbon stocks and biodiversity. *Trends in Ecology and Evolution*, *24*, 541–548.
Cleland, E. E., Chuine, I., Menzel, A., Mooney, H. A., & Schwartz, M. D. (2007). Shifting plant phenology in response to global change. *Trends in Ecology and Evolution*, *22*, 357–365.
Dash, J., Jeganathan, C., & Atkinson, P.M. (2010). The use of MERIS Terrestrial Chlorophyll Index to study spatio-temporal variation in vegetation phenology over India. *Remote Sensing of Environment*, *114*, 1388–1402.
Delbart, N., Picard, G., Toan, T. L., Kergoat, L., Quegan, S., Woodward, I., et al. (2008). Spring phenology in boreal Eurasia over a nearly century time scale. *Global Change Biology*, *14*, 603–614.
Drobot, S. D., & Anderson, M. R. (1999). Interannual variations in snow onset and links to 500 hPa atmospheric anomalies over the Arctic. *Interactions between the cryosphere, climate and greenhouse gases*, *256*, 55–61.
Fitter, A. H., & Fitter, R. S. R. (2002). Rapid changes in flowering time in British plants. *Science*, *296*, 1689–1691.
Forbes, B. C., Fauria, M. M., & Zetterberg, P. (2010). Russian arctic warming and greening are closely tracked by tundra shrub willows. *Global Change Biology*, *16*, 1542–1554.
Geerken, R. A. (2009). An algorithm to classify & monitor seasonal variations in vegetation phenologies & their inter-annual change. *ISPRS Journal of Photogrammetry and Remote Sensing*, *64*, 422–431.
Gong, D. Y., & Ho, C. H. (2003). Detection of large-scale climate signals in spring vegetation index (normalized difference vegetation index) over the Northern Hemisphere. *Journal of Geophysical Research*, *108*, 4498, http://dx.doi.org/10.1029/2002JD002300.
Gouveia, C., Trigo, R. M., DaCamara, C. C., Libonati, R., & Pereira, J. M. C. (2008). The North Atlantic Oscillation and European vegetation dynamics. *International Journal of Climatology*, *28*, 1835–1847.
Hansen, M. C., Defries, R. S., Townshend, J. R. G., & Sohlberg, R. (2000). Global land cover classification at 1 km resolution using a decision tree classifier. *International Journal of Remote Sensing*, *21*, 1331–1365.
Hansen, J., Ruedy, R., Sato, M., & Lo, K. (2010). Global surface temperature change. *Reviews of Geophysics*, *48*, RG4004, http://dx.doi.org/10.1029/2010RG000345.
Hansen, M. C., Stehman, S. V., & Potapov, P. V. (2010). Quantification of global gross forest cover loss. *PNAS*, *107*, 8650–8655.
Hughes, L. (2000). Biological consequences of global warming: Is the signal already? *Trends in Ecological Evolution*, *15*, 56–61.
Hurrell, J. W., & van Loon, H. (1997). Decadal variations in climate associated with the North Atlantic Oscillation. *Climatic Change*, *36*, 301–326.
Jackson, M. T. (1966). Effects of microclimate on spring flowering phenology. *Ecology*, *47*(3), 407–415.
Jakubauskas, M. E., Legates, D. R., & Kastens, J. H. (2001). Harmonic analysis of time-series AVHRR NDVI data. *Photogrammetric Engineering and Remote Sensing*, *67*, 461–470.
Jeganathan, C., Dash, J., & Atkinson, P.M. (2010). Characterising the spatial pattern of phenology for the tropical vegetation of India using multi-temporal MERIS chlorophyll data. *Landscape Ecology*, *25*, 1125–1141.
Jeganathan, C., Dash, J., & Atkinson, P.M. (2010). Mapping the phenology of natural vegetation in India using a remote sensing-derived chlorophyll index. *International Journal of Remote Sensing*, *31*, 5777–5796.
Jeong, S. J., Ho, C. H., Gim, H. J., & Brown, M. E. (2011). Phenology shifts at start vs. end of growing season in temperate vegetation over the Northern Hemisphere for the period 1982–2008. *Global Change Biology*, *17*, 2385–2399.
Julien, Y., & Sobrino, J. A. (2009). Global land surface phenology trends from GIMMS database. *International Journal of Remote Sensing*, *30*, 3495–3513.
Karlsen, S. R., Hogda, K. A., Wielgolaski, F. E., Tolvanen, A., Tommervik, H., Poikolainen, J., et al. (2009). Growing-season trends in Fennoscandia 1982–2006, determined from satellite and phenology data. *Climate Research*, *39*, 275–286.
Keeling, C. D., Chin, J. F. S., & Whorf, T. P. (1996). Increased activity of northern vegetation inferred from atmospheric CO_2 measurements. *Nature*, *382*, 146–149.
Knorr, W., Kaminski, T., Scholze, M., Gobron, N., Pinty, B., & Giering, R. (2010). Carbon cycle data assimilation with a generic phenology model. *Journal of Geophysical Research: Biogeosciences (2005–2012)*, *115*(G4).
Korner, C., & Basler, D. (2010). Phenology under global warming. *Science*, *327*(5972), 1461–1462, http://dx.doi.org/10.1126/science.1186473.
Kross, A., Fernandes, R., Seaquist, J., & Beaubien, E. (2011). The effect of the temporal resolution of NDVI data on season onset dates and trends across Canadian broadleaf forests. *Remote Sensing of Environment*, *115*, 1564–1575.
Latifovic, R., & Pouliot, P. (2007). Analysis of climate change impacts on lake ice phenology in Canada using the historical satellite data record. *Remote Sensing of Environment*, *106*, 492–507.
Linderholm, H. W. (2006). Growing season changes in the last century. *Agricultural and Forest Meteorology*, *137*, 1–14.
Mao, J., Xiaoying, S., Peter, E. T., Piao, S., & Wang, X. (2012). Causes of spring vegetation growth trends in the northern mid-high latitudes from 1982 to 2004. *Environmental Research Letters*, *7*, 014010, http://dx.doi.org/10.1088/1748-9326/7/1/014010.
McPhaden, M. J. (1999). Genesis and evolution of the 1997–98 El Niño. *Science*, *283*, 950–954.
Menzel, A., & Fabian, P. (1999). Growing season extended in Europe. *Nature*, *297*, 659.
Menzel, A., Sparks, T. H., Estrella, N., & Eckhardt, S. (2005). SSW-to-NNE North Atlantic oscillation affects the progress of seasons across Europe. *Global Change Biology*, *11*, 909–918.
Menzel, A., Sparks, T. H., Estrella, N., Koch, E., Aasa, A., Ahas, R., et al. (2006). European phenological response to climate change matches the warming pattern. *Global Change Biology*, *12*, 1969–1976.
Moody, A., & Johnson, D. (2001). Land-surface phenologies from AVHRR using the discrete Fourier transform. *Remote Sensing of Environment*, *75*, 305–323.
Morisette, J. T., Richardson, A. D., Knapp, A. K., Fisher, J. I., Graham, E. A., Abatzoglou, J., et al. (2009). Tracking the rhythm of the seasons in the face of global change: Phenological research in the 21st century. *Frontiers in Ecology and the Environment*, *7*(5), 253–260.
Myneni, R. B., Keeling, C. D., Tucker, C. J., Asrar, G., & Nemani, R. R. (1997). Increased plant growth in the northern high latitudes from 1981–1991. *Nature*, *386*, 698–702.
Nemani, R. R., Keeling, C. D., Hashimoto, H., Jolly, W. M., Piper, S. C., Tucker, C. J., et al. (2003). Climate driven increases in global terrestrial net primary production from 1982 to 1999. *Science*, *300*, 1560–1563.
Parmesan, C., & Yohe, G. (2003). A globally coherent fingerprint of climate change impacts across natural systems. *Nature*, *421*, 37–42.
Penuelas, J., & Filella, L. (2001). Responses to a warming world. *Science*, *294*, 793–795.
Piao, S., Friedlingstein, P., Ciais, P., Zhou, L., & Chen, A. (2006). Effect of climate and CO_2 changes on the greening of the northern hemisphere over the past two decades. *Geophysical research letters*, *33*(L23402), http://dx.doi.org/10.1029/2006GL028205.
Piao, S., Wang, X., Ciais, P., Zhu, B., Wang, T., & Liu, J. (2011). Changes in satellite-derived vegetation growth trend in temperate and boreal Eurasia from 1982 to 2006. *Global Change Biology*, *17*, 3228–3239.
Pinzon, J. (2002). *Using HHT to successfully uncouple seasonal and interannual components in remotely sensed data*. SCI 2002 Conference Proceedings, Jul 14–18. Orlando, Florida.
Pinzon, J., Brown, M. E., & Tucker, C. J. (2004). Satellite time series correction of orbital drift artifacts using empirical mode decomposition. In N. E. Huang, & S. S. P. Shen (Eds.), *EMD and its applications, Vol. 10.* (pp. 285–295). Singapore: World Scientific.
Randerson, J. T., Hoffman, F. M., Thornton, P. E., Mahowald, N. M., Lindsay, K., Lee, Y. H., et al. (2009). Systematic assessment of terrestrial biogeochemistry in coupled climate–carbon models. *Global Change Biology*, *15*, 2462–2484.
Richardson, A. D., Anderson, R. S., Arain, M. A., Barr, A. G., Bohrer, G., Chen, G., et al. (2012). Terrestrial biosphere models need better representation of vegetation phenology: Results from the North American Carbon Program Site Synthesis. *Global Change Biology*, *18*, 566–584.
Roerink, G. J., Menenti, M., & Verhoef, W. (2000). Reconstructing cloud free NDVI composites using Fourier analysis of time series. *International Journal of Remote Sensing*, *21*, 1911–1917.
Rotschky, G., Schuler, T. V., Haarpaintner, J., Kohler, J., & Isaksson, E. (2011). Spatio-temporal variability of snowmelt across Svalbard during the period 2000–08 derived from QuikSCAT/SeaWinds scatterometry. *Polar Research*, *30*, 5963, http://dx.doi.org/10.3402/polar.v30i0.5963.

Stockli, R., & Vidale, P. L. (2004). European plant phenology and climate as seen in a 20-year AVHRR land-surface parameter dataset. *International Journal of Remote Sensing*, *25*, 3303–3330.

Stolbovoi, V. (1999). Classification of Russia's boreal forest in relation to global climate warming. In S. Woxhott (Ed.), *Proceedings of the ninth IBFRA Conference* (pp. 60–69) (September 21–23, Aktuelt, 4, North institute for Skogforskning, Oslo).

Stolbovoi, V. (2006). Soil carbon in the forests of Russia. *Mitigation and Adaptation Strategies for Global Change*, *11*, 203–222.

Tanja, S., Berninger, F., Vesala, T., Markkanen, T., Hari, P., Makela, A., et al. (2003). Air temperature triggers the recovery of evergreen boreal forest photosynthesis in spring. *Global Change Biology*, *9*, 1410–1426.

Thuiller, W., Lavorel, S., Araujo, M. B., Sykes, M. T., & Prentice, I. C. (2005). Climate change threats to plant diversity in Europe. *PNAS*, *102*, 8245–8250.

Tucker, C. J., Fung, I. Y., Keeling, C. D., & Gammon, R. H. (1986). Relationship between atmospheric CO_2 variations and a satellite-derived vegetation index. *Nature*, *319*(16), 195–199.

Tucker, C. J., Pinzon, J. E., Brown, M. E., Slayback, D. A., Pak, E. W., & Mahoney, R. (2005). An extended AVHRR 8-km NDVI data set compatible with MODIS and SPOT vegetation NDVI data. *International Journal of Remote Sensing*, *26*, 4485–4498.

Verbyla, D. (2008). The greening and browning of Alaska based on 1982–2003 satellite data. *Global Ecology and Biogeography*, *17*, 547–555.

Verhoef, W., Menenti, M., & Azzali, S. (1996). A colour composite of NOAA-AVHRRNDVI based on time series (1981–1992). *International Journal of Remote Sensing*, *17*, 231–235.

Vitasse, Y., Francois, C., Delpierre, N., Dufrene, E., Kremer, A., Chuine, I., et al. (2011). Assessing the effects of climate change on the phenology of European temperate trees. *Agricultural and Forest Meteorology*, *151*, 969–980.

Wagenseil, H., & Samimi, C. (2006). Assessing spatio-temporal variations in plant phenology using Fourier analysis on NDVI time series: Results from a dry savannah environment in Namibia. *International Journal of Remote Sensing*, *27*, 3455–3471.

Wang, X. H., Piao, S. L., Ciais, P., Li, J., Friedlingstein, P., Koven, C., et al. (2011). Spring temperature change and its implication in the change of vegetation growth in North America from 1982 to 2006. *PNAS*, *108*(4), 1240–1245.

Weeks, J. R. (2012). *Population: An introduction to concepts and issues.* Wadsworth: Cengage Learning (ISBN-13: 978-1-111-18597-8, Belmont, CA, USA).

White, M. A., deBeurs, K. M., Didan, K., Inouye, D. W., Richardson, A. D., & Jensen, O. P. (2009). Intercomparison, interpretation, & assessment of spring phenology in North America estimated from remote sensing for 1982–2006. *Global change biology*, *15*, 2335–2359.

Xu, L., Myneni, R. B., Chapin, F. S., Callaghan, T. V., Pinzon, J. E., Tucker, C. J., et al. (2013). Temperature and vegetation seasonality diminishment over northern lands. *Nature Climate Change Letters*, *3*, 581–586, http://dx.doi.org/10.1038/nclimate1836.

Zhang, N., Yasunari, T., & Ohta, T. (2011). Dynamics of the larch taiga–permafrost coupled system in Siberia under climate change. *Environmental Research Letters*, *6*, http://dx.doi.org/10.1088/1748-9326/6/2/024003.